AD-A232 006

Double-Crystal X-Ray Diffraction Studies of Si Ion-Implanted Laser-Annealed GaAs

Prepared by

P. M. ADAMS
Materials Sciences Laboratory
Laboratory Operations

DTIC
ELECTE
FEB 19 1991
S B D

8 January 1991

Prepared for

SPACE SYSTEMS DIVISION
AIR FORCE SYSTEMS COMMAND
Los Angeles Air Force Base
P. O. Box 92960
Los Angeles, CA 90009-2960

Engineering and Technology Group

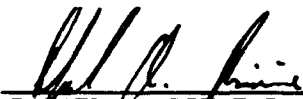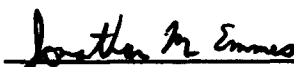THE AEROSPACE CORPORATION
El Segundo, California

91 2 11 119

This report was submitted by The Aerospace Corporation, El Segundo, CA 90245-4691, under Contract No. F04701-88-C-0089 with the Space Systems Division, P.O. Box 92960, Los Angeles, CA 90009-2960. It was reviewed and approved for The Aerospace Corporation by S. Feuerstein, Director, Materials Sciences Laboratory. Captain Riviere was the project officer for the Mission-Oriented Investigation and Experimentation (MOIE) program.

This report has been reviewed by the Public Affairs Office (PAS) and is releasable to the National Technical Information Service (NTIS). At NTIS, it will be available to the general public, including foreign nationals.

This technical report has been reviewed and is approved for publication. Publication of this report does not constitute Air Force approval of the report's findings or conclusions. It is published only for the exchange and stimulation of ideas.

RAFAEL A. RIVIERE, Capt, USAF
MOIE Project Officer
SSD/CNL

JONATHAN M. EMMES, Maj, USAF
MOIE Program Manager
STC/WCO OL-AB

REPORT DOCUMENTATION PAGE

1a. REPORT SECURITY CLASSIFICATION Unclassified	1b. RESTRICTIVE MARKINGS
2a. SECURITY CLASSIFICATION AUTHORITY 2b. DECLASSIFICATION/DOWNGRADING SCHEDULE	3. DISTRIBUTION/AVAILABILITY OF REPORT Approved for public release; distribution unlimited.
4. PERFORMING ORGANIZATION REPORT NUMBER(S) TR-0090(5945-07)-2	5. MONITORING ORGANIZATION REPORT NUMBER(S) SSD-TR-90-57

6a. NAME OF PERFORMING ORGANIZATION The Aerospace Corporation Laboratory Operations	6b. OFFICE SYMBOL (If applicable)	7a. NAME OF MONITORING ORGANIZATION Space Systems Division
6c. ADDRESS (City, State, and ZIP Code) El Segundo, CA 90245-4691		7b. ADDRESS (City, State, and ZIP Code) Los Angeles Air Force Base Los Angeles, CA 90009-2960
8a. NAME OF FUNDING/SPONSORING ORGANIZATION	8b. OFFICE SYMBOL (If applicable)	9. PROCUREMENT INSTRUMENT IDENTIFICATION NUMBER F04701-88-C-0089

8c. ADDRESS (City, State, and ZIP Code)	10. SOURCE OF FUNDING NUMBERS			
	PROGRAM ELEMENT NO.	PROJECT NO.	TASK NO.	WORK UNIT ACCESSION NO.

11. TITLE (Include Security Classification)

Double Crystal X-Ray Diffraction Studies of Si Ion-Implanted Laser-Annealed GaAs

12. PERSONAL AUTHOR(S)
Adams, Paul M.

13a. TYPE OF REPORT	13b. TIME COVERED FROM _____ TO _____	14. DATE OF REPORT (Year, Month, Day) 1991 January 08	15. PAGE COUNT 42

16. SUPPLEMENTARY NOTATION·

17. COSATI CODES			18. SUBJECT TERMS (Continue on reverse if necessary and identify by block number)
FIELD	GROUP	SUB-GROUP	Rocking Curves X-Ray Diffraction X-Ray Topographs Ion-Implantation Laser Annealing

19. ABSTRACT (Continue on reverse if necessary and identify by block number)

Double-crystal x-ray rocking curves and topographs have been used to study the relief of strain produced by pulsed laser annealing in $^{28}Si^+$ ion-implanted GaAs. X-ray rocking curves of 140 keV $2 \times 10^{14}/cm^2$ as-implanted GaAs indicated that the upper 2500 Å of the sample had been strained to a maximum of 0.38%. Rocking curves from two of the single-shot laser anneal sites with the highest energy densities (and largest areas of annealing) indicated that the ion-implantation strain had been almost completely relieved. X-ray rocking curves of the 180 keV $5 \times 10^{15}/cm^2$ as-implanted GaAs revealed that the surface of the sample had been strained to a depth of 6000 Å with a maximum strain of 0.50%. Rocking curves from rastered laser anneal sites indicated that considerable strain remained in the sample.

20. DISTRIBUTION/AVAILABILITY OF ABSTRACT ☒ UNCLASSIFIED/UNLIMITED ☐ SAME AS RPT. ☐ DTIC USERS	21. ABSTRACT SECURITY CLASSIFICATION Unclassified
22a. NAME OF RESPONSIBLE INDIVIDUAL	22b. TELEPHONE (Include Area Code) 22c. OFFICE SYMBOL

DD FORM 1473, 84 MAR   83 APR edition may be used until exhausted.   SECURITY CLASSIFICATION OF THIS PAGE
All other editions are obsolete

UNCLASSIFIED

19. ABSTRACT (Continued)

Double-crystal reflection x-ray topographs of the $2 \times 10^{14}/cm^2$ implanted sample, taken at various positions on the rocking curve, were able to qualitatively map out the state of strain in the whole surface of the sample to much higher resolution than the x-ray rocking curves. Laser energy densities of greater than approximately 0.25 J/cm^2 were able to relieve nearly all of the ion-implantation strain in at least some portion of each site, whereas all laser energy densities were able to relieve strains of above 0.21% in some portions of each site. The x-ray topographs of the laser sites exhibited unusual interference fringe patterns that have been attributed to a bi-crystal structure produced in some areas of the laser-annealed areas. The results of x-ray topographs of the $5 \times 10^{15}/cm^2$ sample agreed with the x-ray rocking curves and revealed the presence of residual strains.

ACKNOWLEDGMENTS

Accession For	
NTIS GRA&I	☑
DTIC TAB	☐
Unannounced	☐
Justification	
By	
Distribution/	
Availability Codes	
Dist	Avail and/or Special
A-1	

CONTENTS

3

FIGURES

FIGURES (Continued)

I. INTRODUCTION

Pulsed laser annealing has been studied as a way of activating surface layers of GaAs that have been heavily doped by ion-implantation (Ref. 1). Double-crystal x-ray diffraction techniques are very sensitive to strains and defects in single crystals and provide a means for characterizing and quantifying the damage produced by ion-implantation and the subsequent relief of the damage by pulsed laser annealing.

Details of the ion-implantation and laser annealing of GaAs are given in References 1 and 2, and the following serves as a summary. Two samples were studied in this investigation. One consisted of a <100> GaAs wafer onto which a 55 nm thick cap of Si_3N_4 was deposited using a pyrolytic decomposition. This Si_3N_4 cap served as a barrier for the volitalization of As during the laser annealings. The capped sample was then ion implanted with $^{28}Si^+$ ions for a total dose of 2×10^{14}/cm^2 at 140 keV. A frequency-doubled Nd:Yag pumped dye laser with a wavelength of 728 nm and a spot size of 200 μm × 450 μm was used to anneal the ion implantion damage. A 5 mm × 8 mm piece of the implanted GaAs was spot annealed in 18 sites with laser energy densities ranging from 0.045 J/cm^2 to 0.9 J/cm^2. Figures 1A and 1B show the as-received annealed specimen. The laser energy densities for the individual sites are given below:

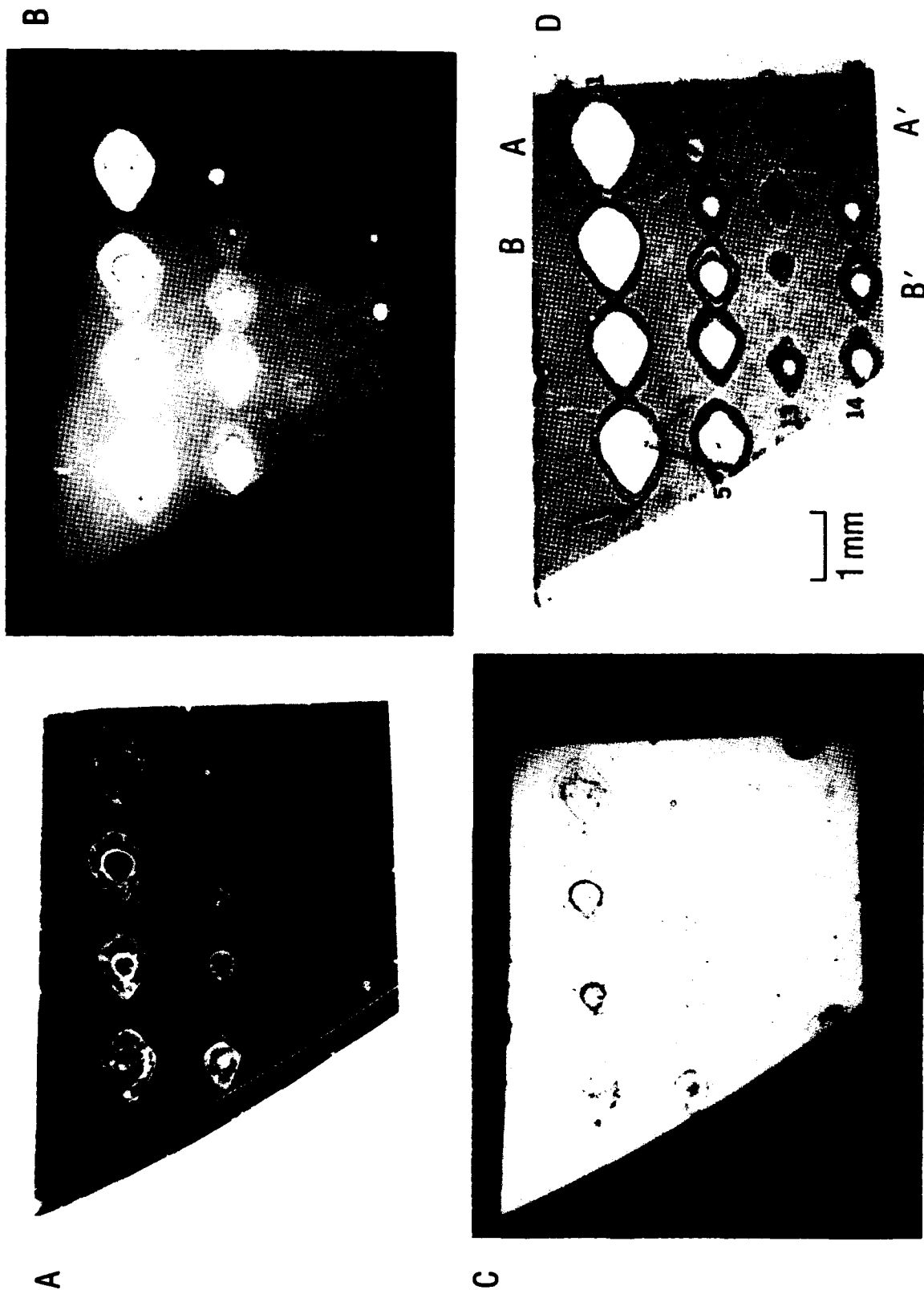| Site	Energy Density (J/cm^2)	Site	Energy Density (J/cm^2)
1	0.9	10	0.07
2	0.7	11	0.06
3	0.5	12	0.045
4	0.7	13	0.045
5	0.36	14	0.06
6	0.25	15	0.12
7	0.18	16	0.09
8	0.09	17	0.08
9	0.12	18	0.06

7

Figure 1. Macrophotographs of As-Received Laser-Annealed GaAs Specimen with Oblique (A) and Normal (B) Incidence Illumination. Figure C shows the specimen with normal incidence illumination after the silicon nitride layer has been removed with HF. Figure D is a (422) reflection double-crystal x-ray topograph exposed at the maximum strain peak.

8

It can be seen from Figure 1B that sites with energy densities of greater than 0.07 J/cm^2 experienced failure of the Si_3N_4 over-layer. The remaining Si_3N_4 was dissolved with hydrofluoric acid since it would interfere with x-ray diffraction analyses. A second sample consisted of a <100> GaAs wafer which had been implanted with $^{28}Si^+$ ions at 180 keV for a total dose of 5 x $10^{15}/cm^2$. This sample was then similarly laser annealed in three areas in a rastered fashion (4 x 11 spots) to provide a larger annealed area (~ 1 x 2 mm). The laser energy densities associated with the three annealed sites were:

Site 1   0.69 J/cm^2

Site 2   0.27 J/cm^2

Site 3   0.12 J/cm^2

The two samples will subsequently be distinguished by referring to whether they were spot or raster annealed.

Several of the spot-annealed laser sites that had lost the Si_3N_4 over-layer displayed ring-like features that were suspected of being craters. For this reason, profilometer traces were recorded across four of the sites (Figure 2). The scans were recorded from top to bottom across the specimen as it appears in Figure 1. The prominent rings visible in sites 2 and 3 are defined by ridges up to several thousand Å in height, while the central regions represent depressions up to 1000 Å in depth. Profilometer traces were also attempted on sites 1 and 4. Well defined craters were not observed; however, curvature at the surface in both of these areas made it difficult to obtain good traces. Profilometer scans were also made of sites 6 and 7 (Figures 2C, 2D); the circular features visible in Figure 1 were determined to be ridges. Central depressions were not easily discernable, and if present, must have been less than about 200 Å in depth. Debris or other irregularities on the surface were on the order of about 1000 Å in height.
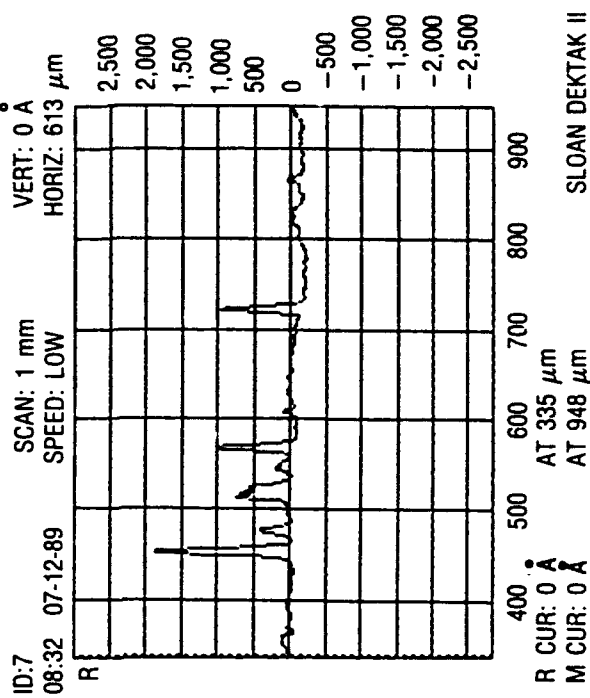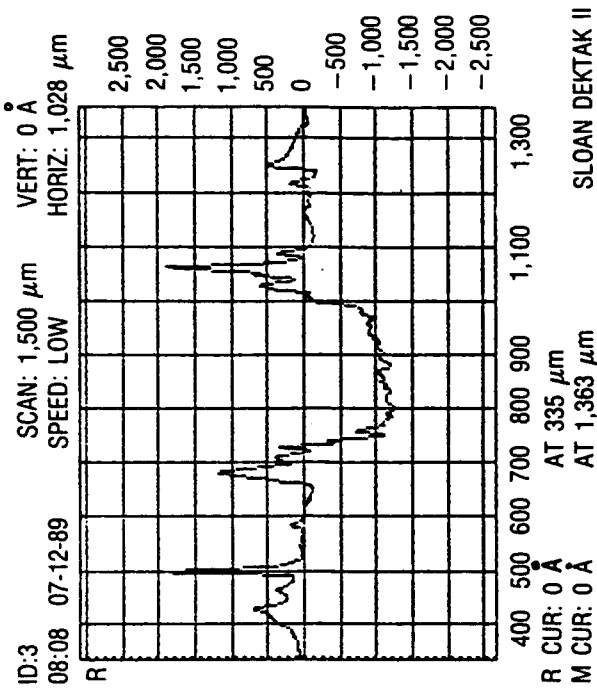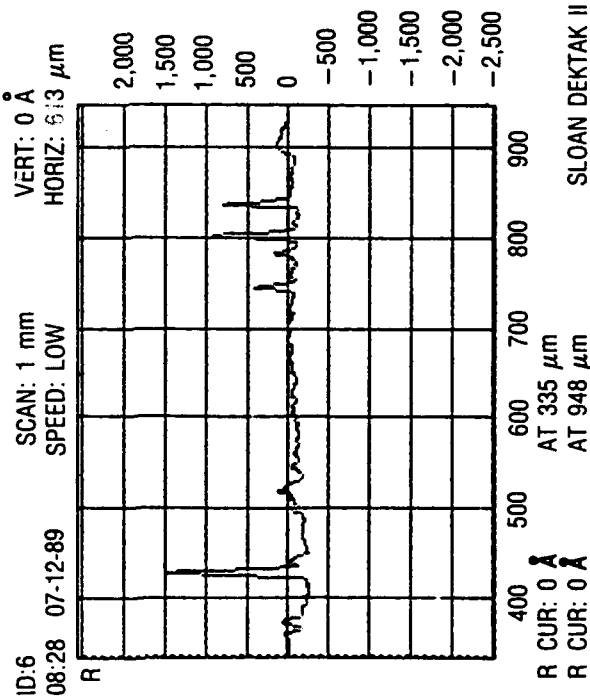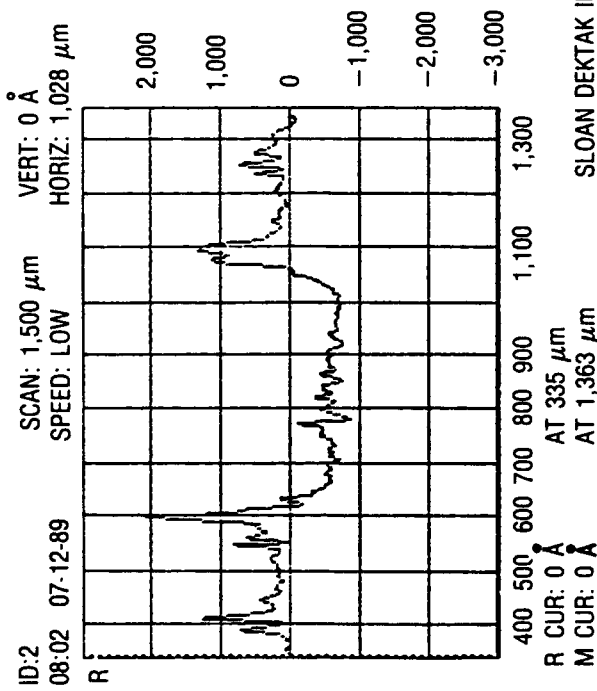
Figure 2. Profilometer Traces Across Laser Anneal Sites 2, 3, 6, and 7. Lateral scale is in microns, vertical scale is in Angstroms.

10

II. DOUBLE-CRYSTAL X-RAY DIFFRACTION ANALYSIS

X-ray rocking curves obtained from a double-crystal diffractometer are extremely sensitive at measuring the strains induced by ion-implantation and have been applied to the study of gallium arsenide and other semi-conductors (Refs. 3-6). The use of a kinematical model of x-ray diffraction allows the determination of strain and disorder depth-profiles from the rocking curves through an iterative procedure (Ref. 7). X-ray rocking curves and x-ray topography have also been used to study the effects of laser and furnace annealing on ion-implanted silicon (Refs. 8-10).

In this study, x-ray rocking curves of the as-implanted and laser-annealed GaAs were obtained with a commercially available (Blake Industries) double-crystal diffractometer using $Cu_{K\alpha 1}$ radiation. A <100> germanium (Ge) crystal aligned for the (400) reflection and a series of slits were used to obtain a 100 μm × 600 μm monochromatic x-ray beam. By translating the specimen with a micrometer, a series of (400) rocking curves were obtained from the GaAs samples at 250 to 625 micron intervals across the laser anneal sites. The specimen was translated parallel to the narrow dimension of the x-ray beam, which corresponds to a distance of 200 μm on the sample due to the 57° angle of incidence.

Double-crystal x-ray topographs were obtained from the samples by aligning the Ge monochromator for the (422) reflection which produces a much larger area of coverage on the sample. For the spot anneal sample, a series of (400) reflection x-ray topographs were obtained at seven positions on the x-ray rocking curve, whereas a single (422) topograph was recorded at the maximum strain peak produced by the ion-implantation. Three (400) reflection x-ray topographs were taken at various positions on the rocking curve of the raster annealed sample. The topographs were recorded on Ilford L-4 nuclear emulsion plates with a 50 μm thick emulsion layer.

11

III. RESULTS

A. SPOT-ANNEALED GaAs

1. X-RAY ROCKING CURVES

Figure 3A presents a (400) rocking curve obtained from an unannealed portion of the ion-implanted GaAs. A rocking curve calculated from a kinematical model of x-ray diffraction (Ref. 7), using the strain and disorder depth profiles in Figure 3B, is shown for comparison. The peaks on the minus delta theta side of the rocking curve are produced by strains from an expansion of the lattice as a result of ion-implantation. The strongest strain peak at ~ -500 arc sec delta theta corresponds to a maximum strain of 0.38%. There are reasonably good matches between the experimental and calculated (400) rocking curves, which indicate that the general shapes of the strain/disorder depth profiles are correct, but the specifics of the profiles may be slightly in error. The strain-depth profile shows that the lattice is strained to a maximum of 0.38% to a depth of approximately 2000 Å and that the strain then decreased to zero over approximately another 1000 Å. It is noted that x-ray rocking curves are not sensitive to amorphous material (hence cannot be modeled), and it is assumed that the dose of the ion-implantation was insufficient to produce complete amorphization.

Twenty-one (400) reflection rocking curves were taken at 250 μm intervals across the sample along lines A-A' and B-B' in Figure 1D, where scans are denoted by prefixes LA and LB, respectively. Scans are numbered from 1 beginning at A' and B', to 21 at A and B. Figures 4A and 4B show rocking curves of unannealed areas along both traverses. The rocking curves all look identical to each other and are similar to that shown in Figure 3. Figure 5 displays the rocking curves of the areas closest to the center of the laser anneal sites for both traverses. It can be seen from the rocking curves of laser sites 1, 2, 7, and 9 that a considerable amount of strain has been relieved as a result of the annealing. This is indicated by the decreased intensities of the strain peaks on the minus delta theta side of the rocking curves. It is noted that the profilometer traces
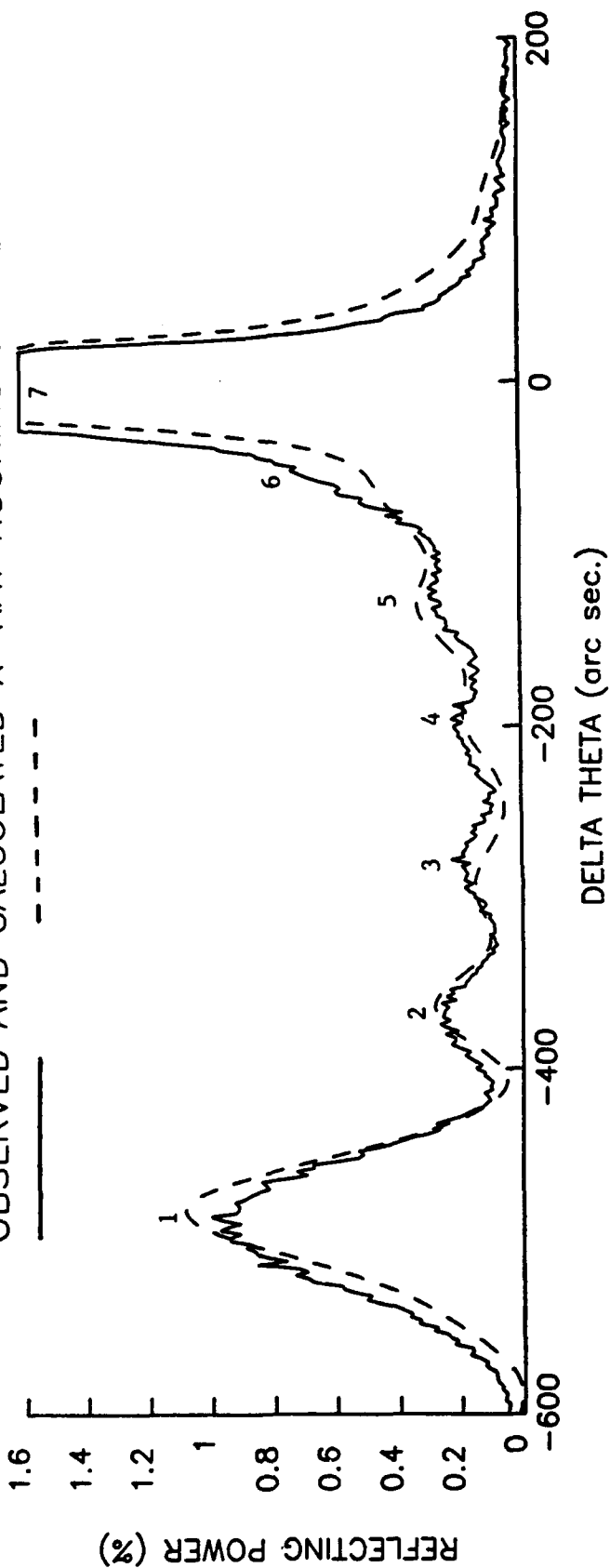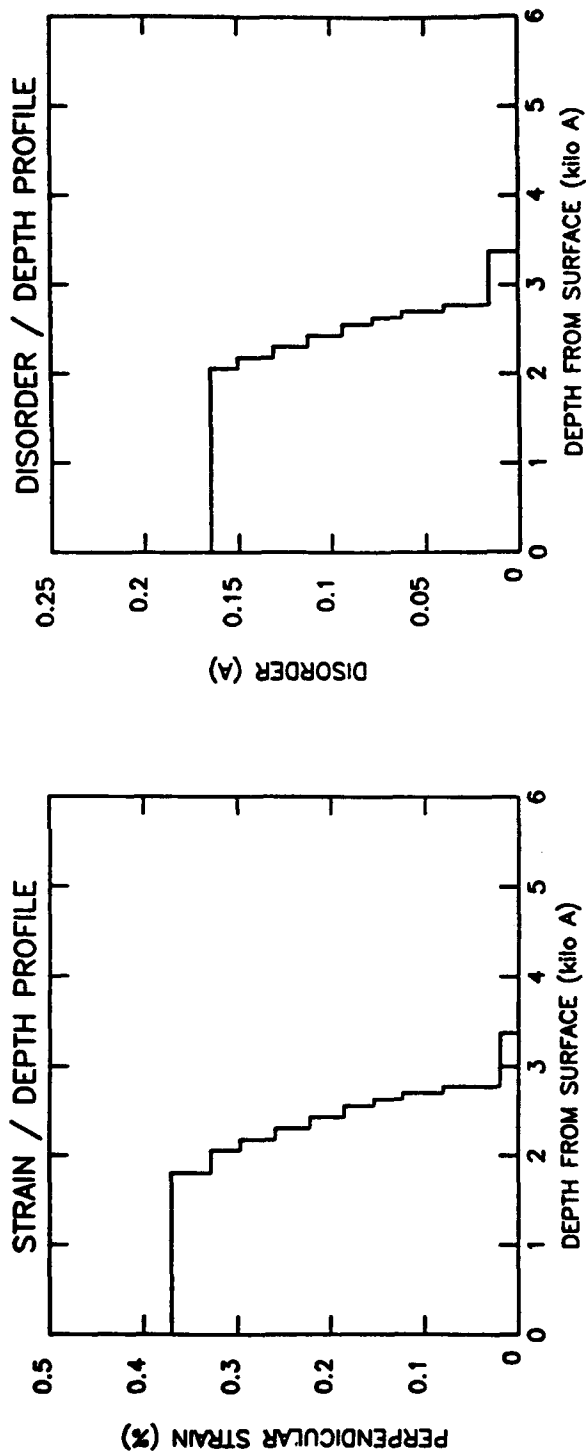
Figure 3A. Experimental and Calculated (400) Rocking Curves of $2 \times 10^{14}/cm^2$ As-Implanted GaAs
Figure 3B. Strain and Disorder Depth Profiles Used to Produce the Calculated Rocking Curve in Figure 3A

Figure 4.   (400) Reflection X-Ray Rocking Curves of Areas Between
            Laser Annealed Sites from Traverses A-A' and B-B'

A

B

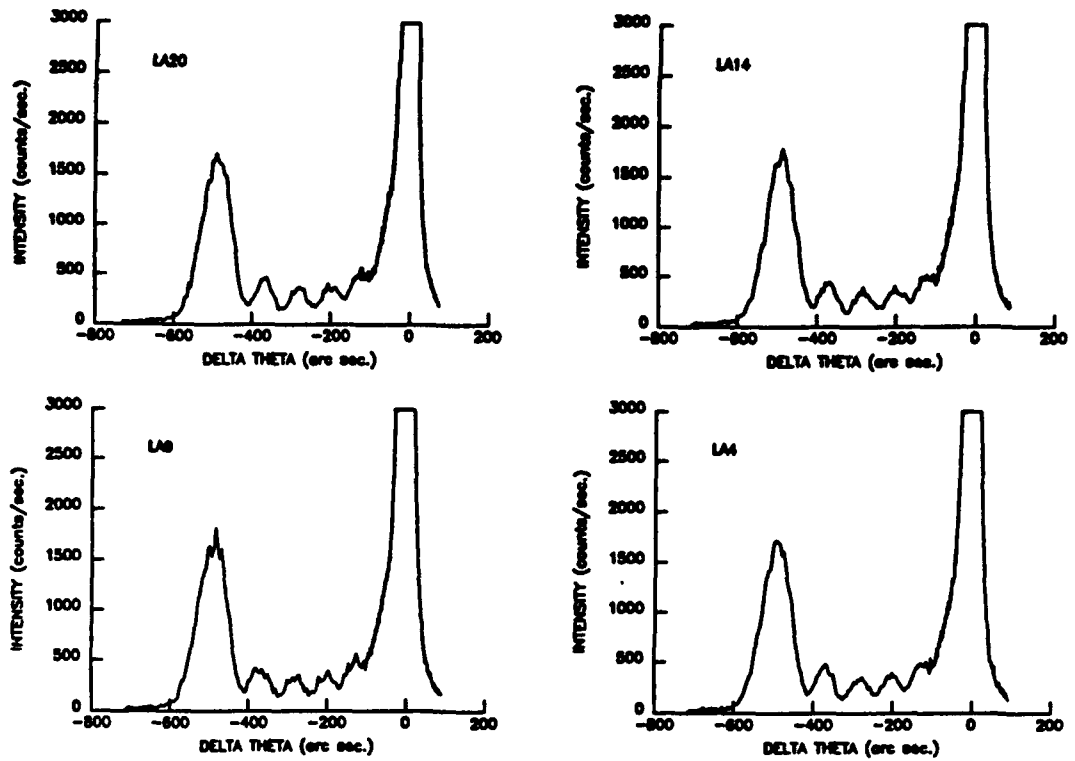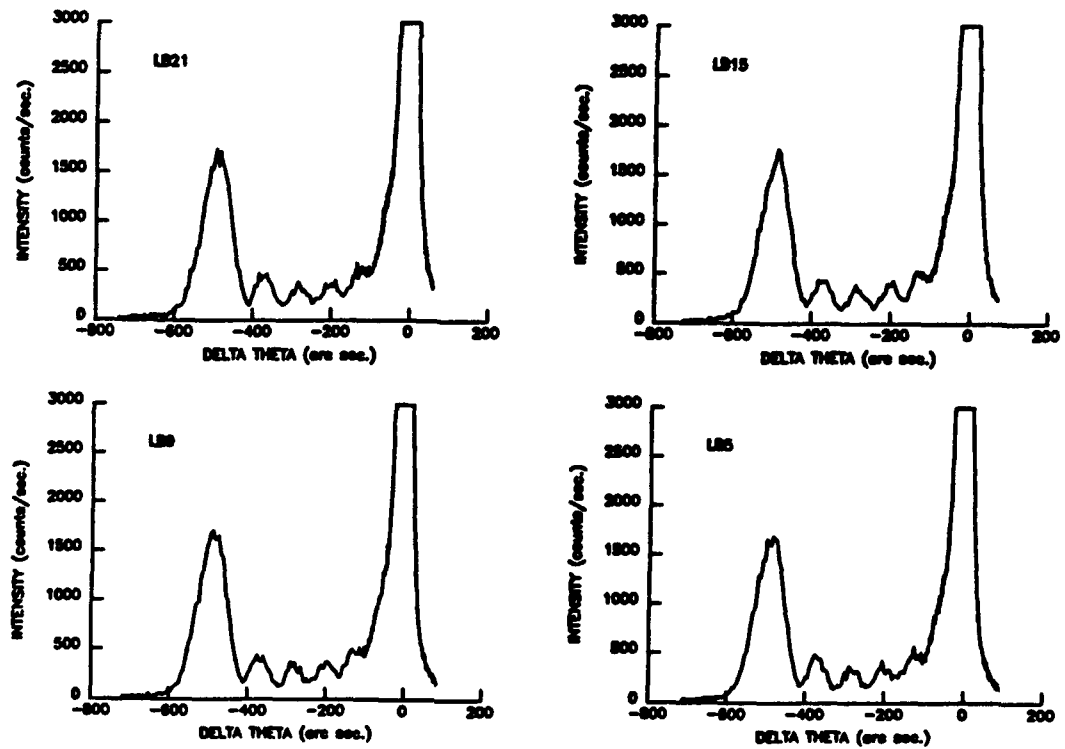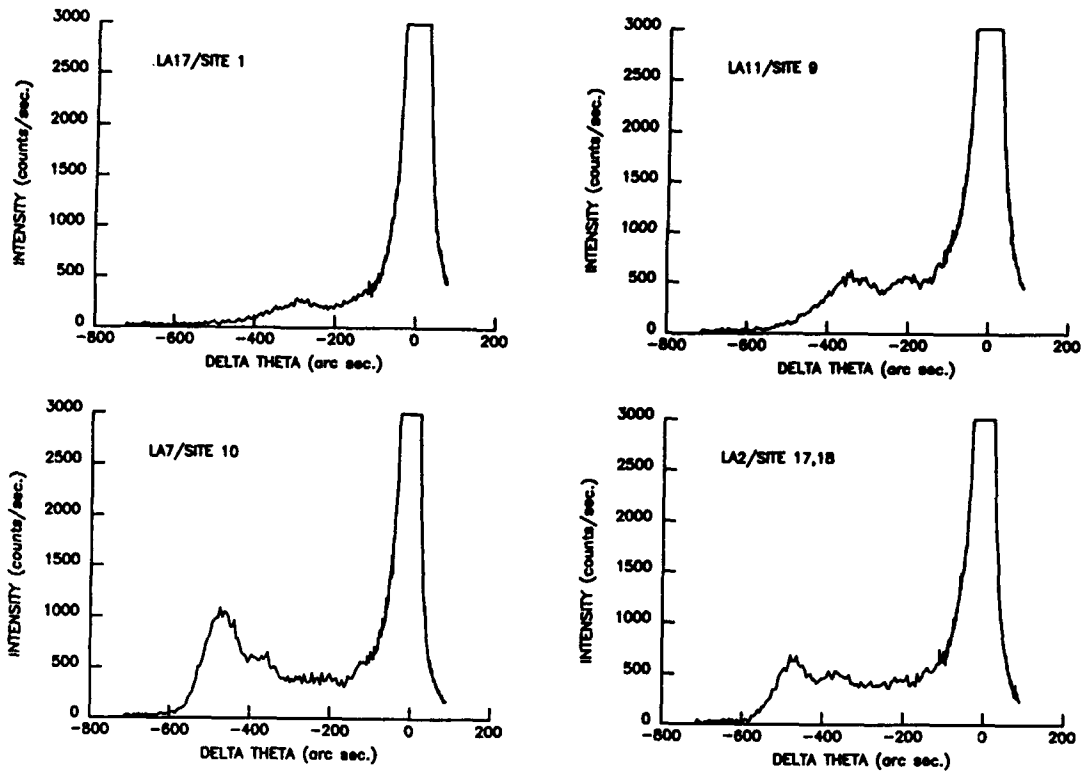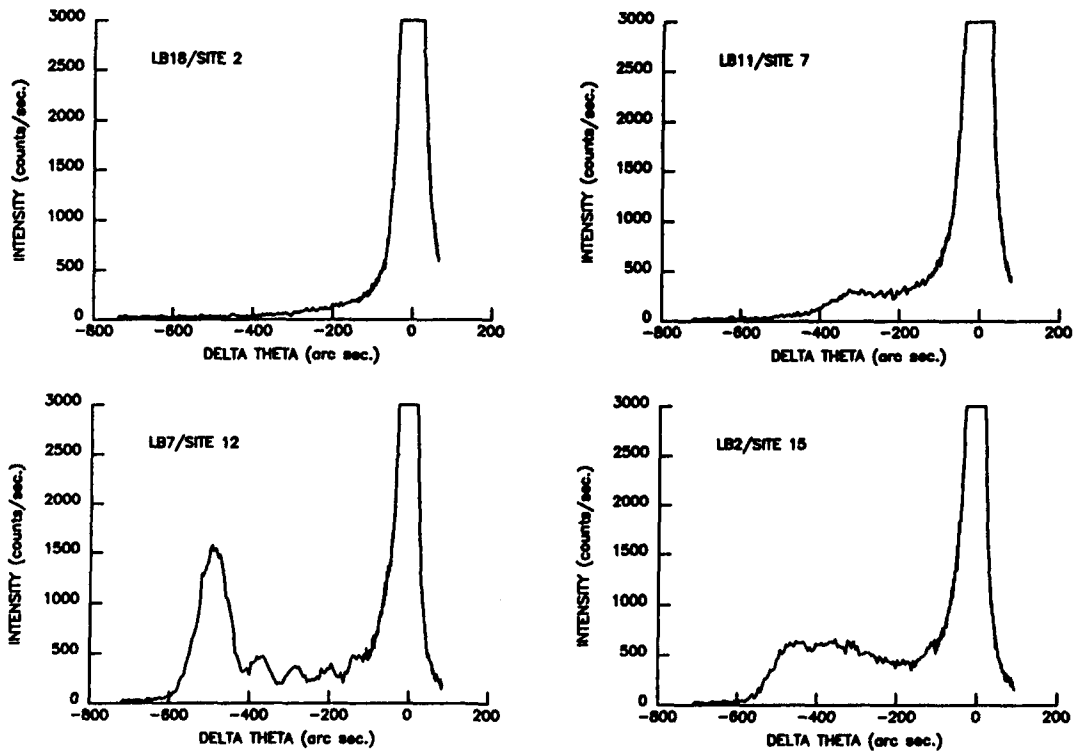Figure 5. (400) Reflection X-Ray Rocking Curves of Laser
Annealed Areas from Traverses A-A' and B-B'

16

of sites 2 and 3 have shown that up to 1000 Å of material has been removed from some of the sites with the highest laser energy densities and that this accounts for up to half the thickness of the most highly strained material (Figure 3B). Material removal may have affected sites 1-5, but profilometer traces of sites 6 and 7 have demonstrated that removal is minimal at sites with lower energy densities. Figure 6 contains rocking curve intensity contour maps compiled from the 21 rocking curves obtained from each traverse, and represents x-ray intensity as a function of position on the sample and delta theta on the rocking curve. Minima in the strain peak intensity contours can be seen at the positions corresponding to the laser anneal sites. Figures 7A and 7B represent psuedo three-dimensional plots of portions of this same data.

Figure 8 presents rocking curve intensity contour maps of the unstrained GaAs substrate for the 21 scans of each of the traverses. It was assumed that laser annealing would relieve the ion-implantion-induced strain, which would result in an increase in the unstrained GaAs peak. No clear trend relating unstrained intensity and annealing, however, is dis-cernable from the intensity contours. This is consistent with preliminary attempts at trying to locate laser sites by monitoring the intensity of the unstrained (400) peak as a function of position on the sample. It was found that areas of maximum intensity didn't necessarily correspond with those of strain relief. It was for this reason that a series of rocking curves were recorded across the sample (Figure 6). This maximized the chances that rocking curves were recorded from the laser-annealed sites. Figures 9 and 10 contain individual rocking curves of the unstrained (400) reflections. Figure 9 shows that rocking curves from both as-implanted and annealed regions are very similar. In Figure 10 unstrained (400) peaks from adjacent areas along traverse B-B' are closely compared. These correspond to the locations at 3.25 mm (LB9) to 1.50 mm (LB16) in Figure 7A. While subtle differences in the intensity and shape of the rocking curves exist, no clear consistent trend between the center of laser site 7 (LB11) and an as-implanted region (LB15) can be found. Therefore, the slight differences in the unstrained (400) peaks are probably due to local variations in the quality of the GaAs substrate.

A

B
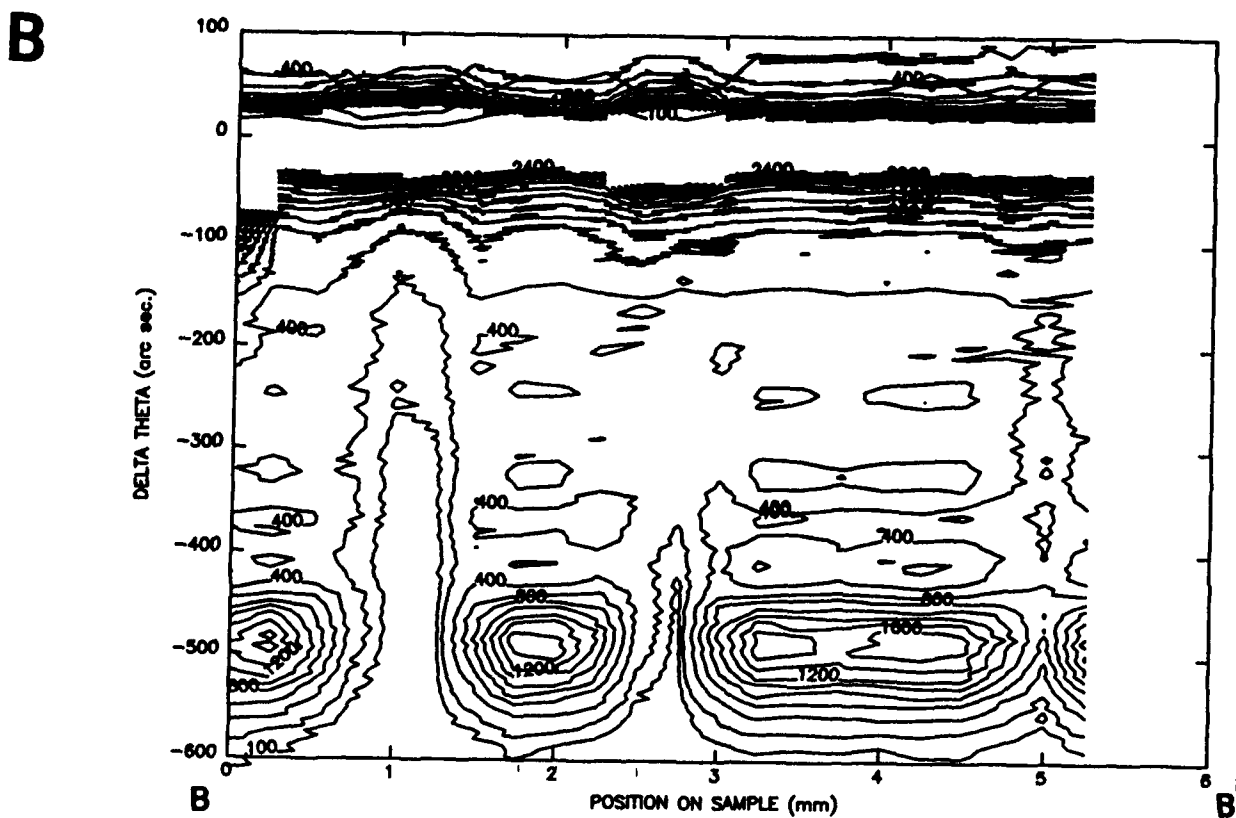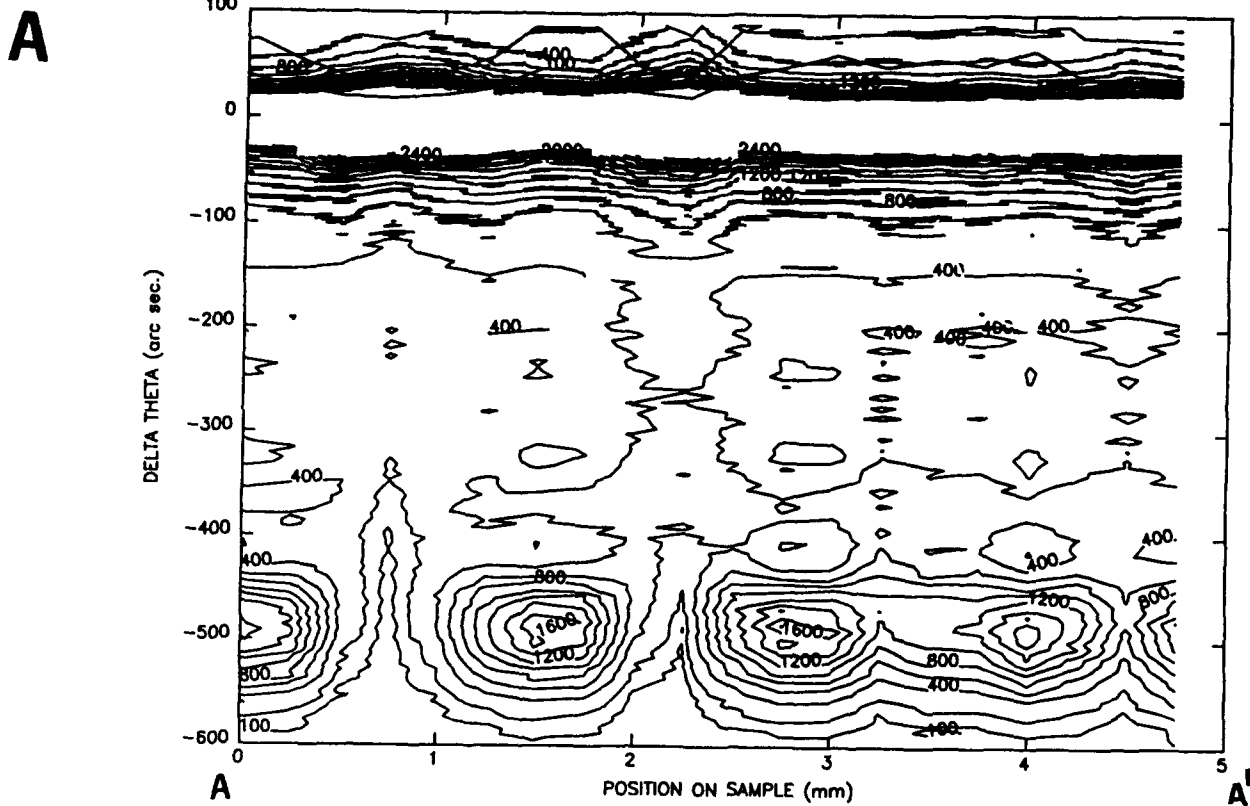
Figure 6. (400) Reflection X-Ray Rocking Curve Intensity
Contour Maps Across Traverses A-A' and B-B'

18
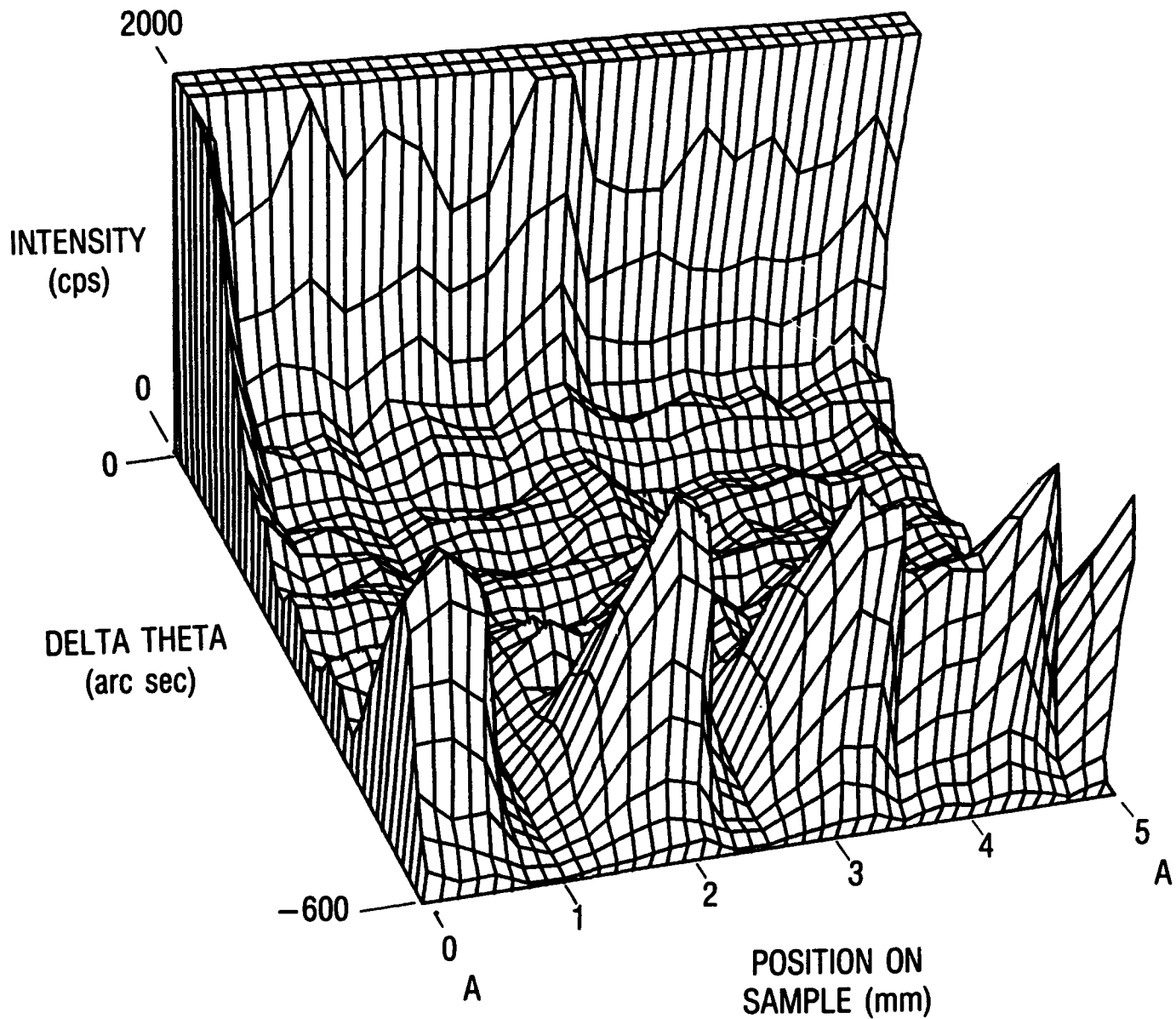
Figure 7A. Pseudo Three-Dimensional Plots of Rocking Curve
Intensities as a Function of Position Across
Traverse A to A'

19
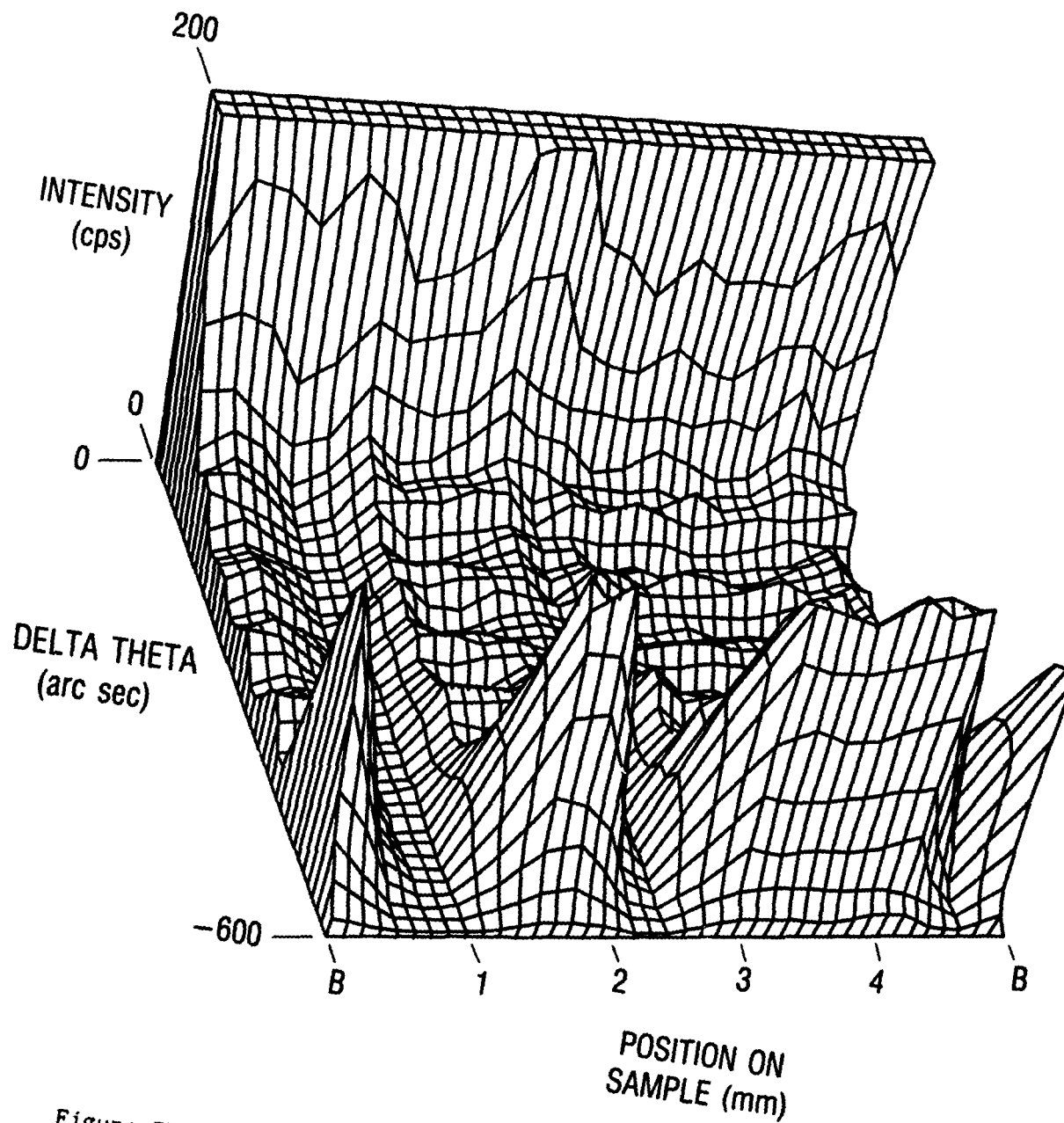
Figure 7B. Pseudo Three-Dimensional Plots of Rocking Curve Intensities as a Function of Position Across Traverse B to B'

20
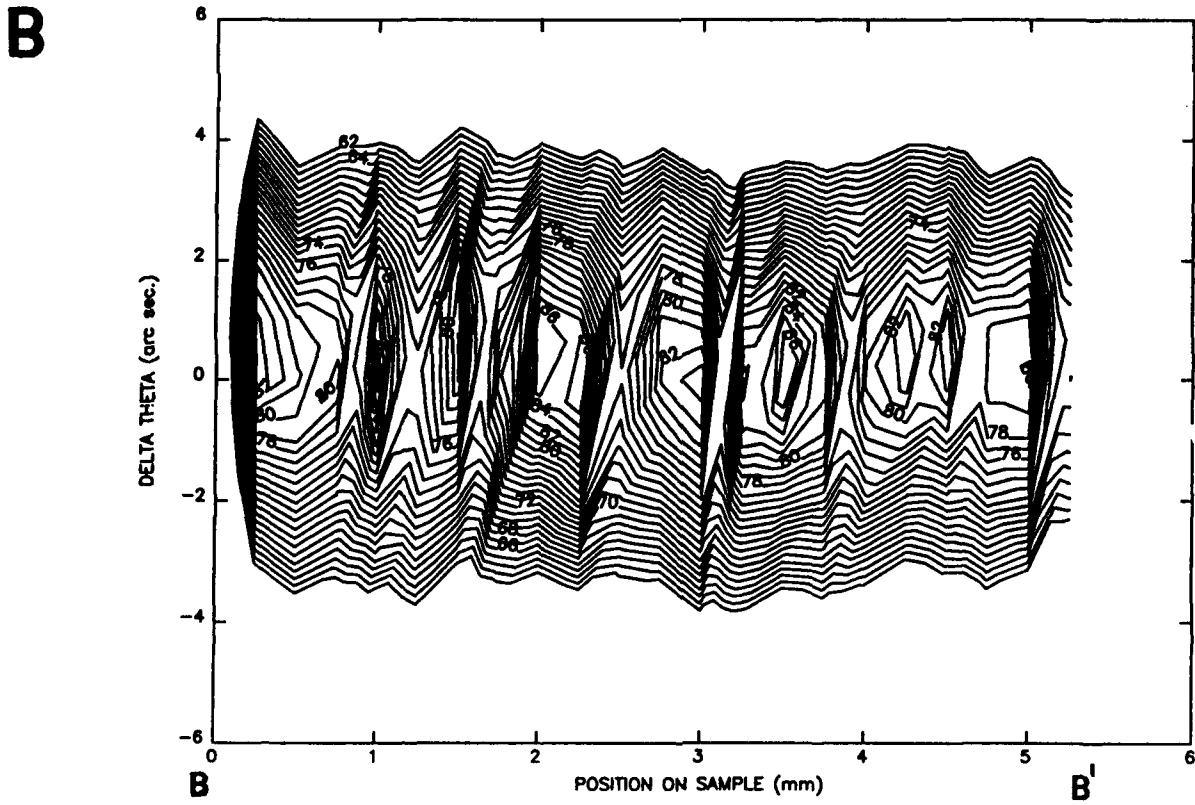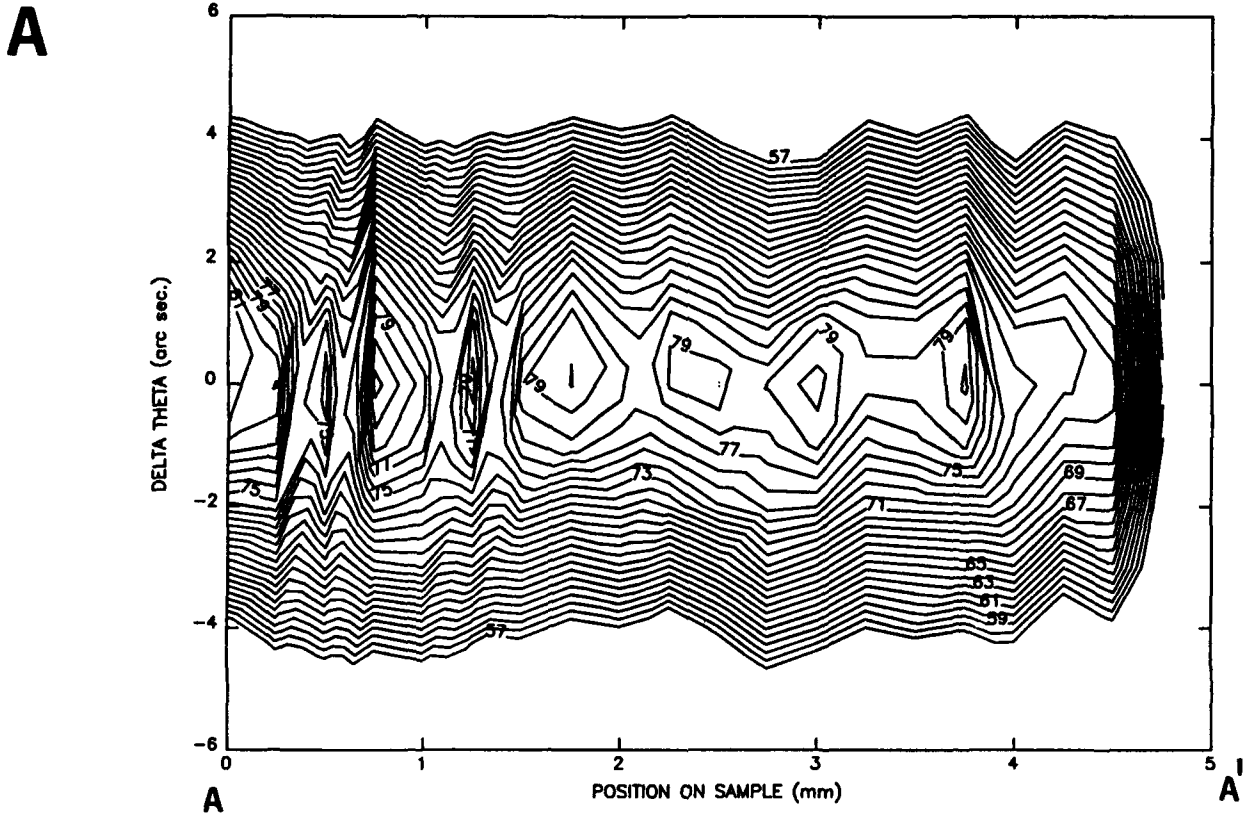
Figure 8. (400) Reflection X-Ray Rocking Curve Intensity Contour Maps for Unstrained GaAs Across Traverses A-A' (A) and B-B' (B). See Figures 9 and 10 for examples of actual rocking curves.

21

A
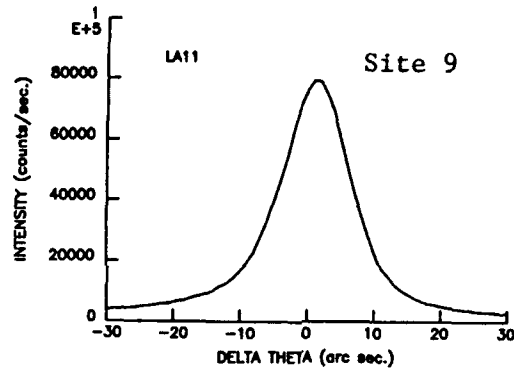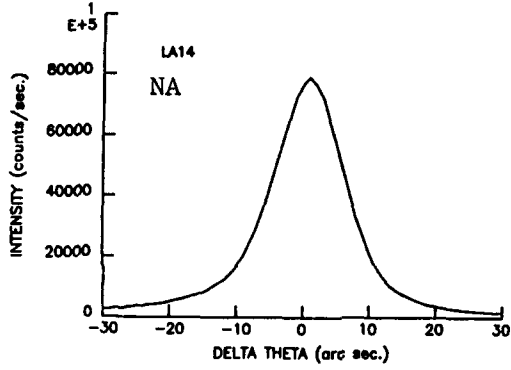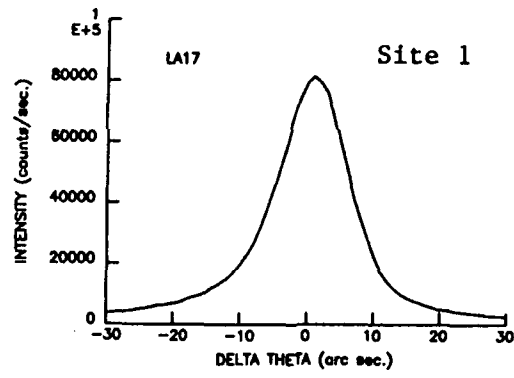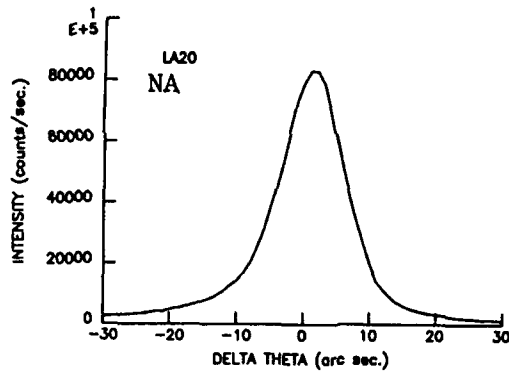
B
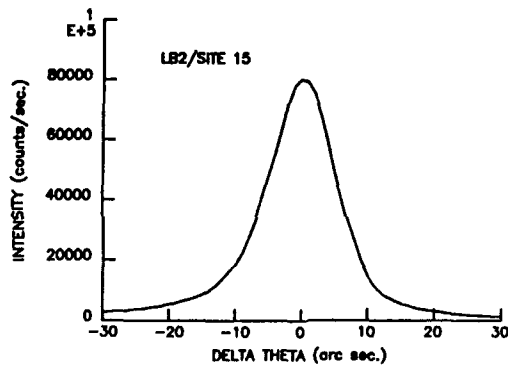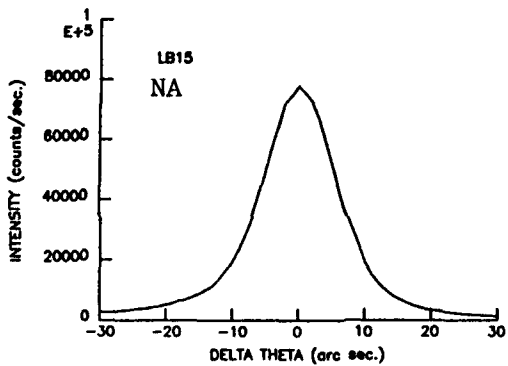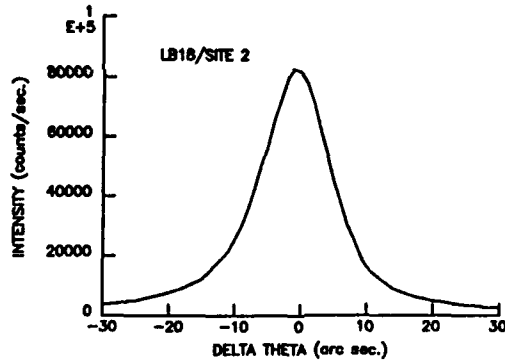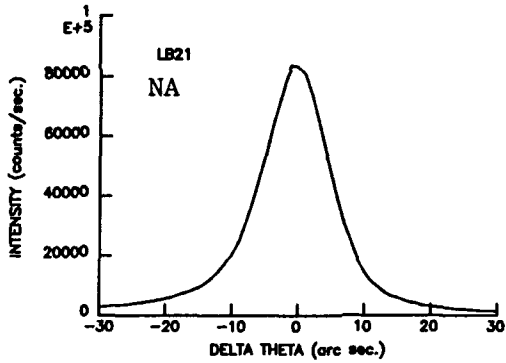
Figure 9. (400) Reflection X-Ray Rocking Curves Along Traverses
A-A' (Sites 1 and 9) and B-B' (Sites 2 and 15). The
rocking curves compare the unstrained GaAs peaks of laser-
annealed and nonannealed (NA) sites.

22
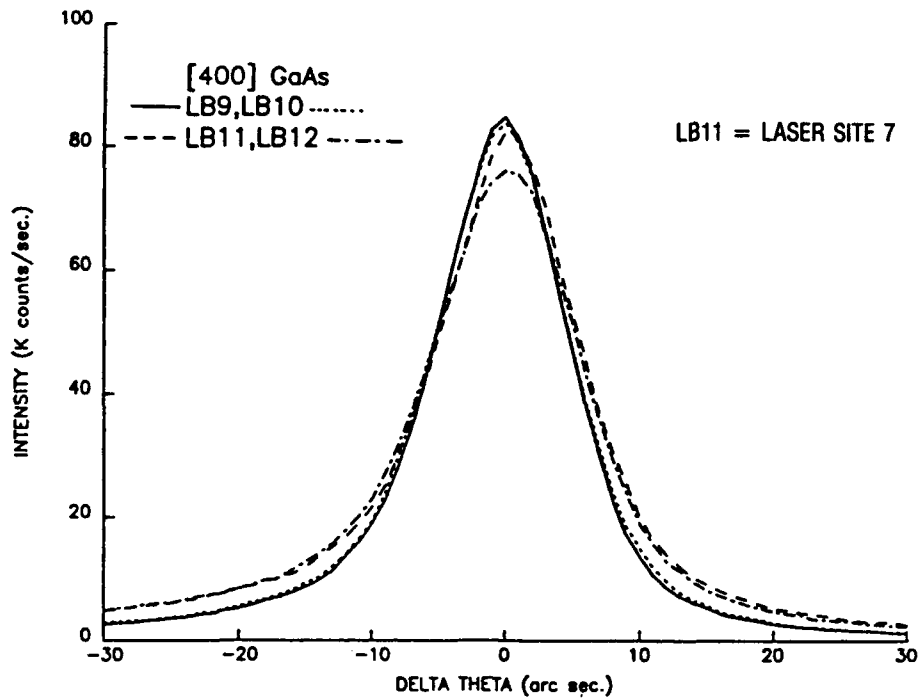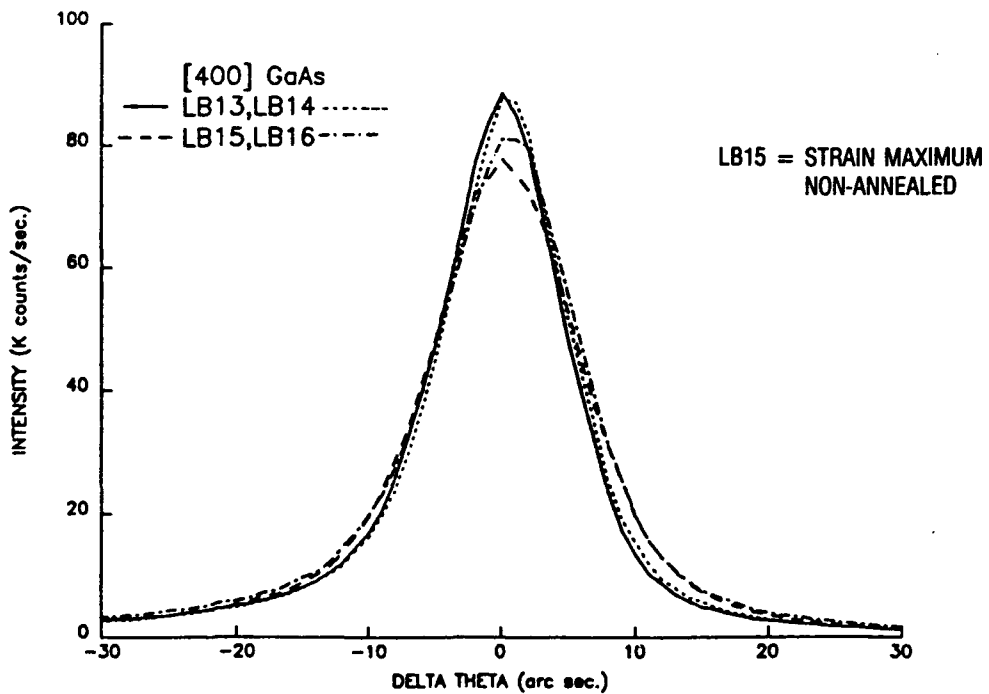
Figure 10. (400) Reflection X-Ray Rocking Curves Along Traverses A-A' (A) and B-B' (B). The rocking curves compare the unstrained GaAs peaks of laser-annealed and nonannealed sites.

2. DOUBLE-CRYSTAL X-RAY TOPOGRAPHY

After preliminary attempts at manually locating the center of laser anneal sites were unsuccessful, it was decided that a reflection x-ray topograph would provide a quick survey of the state of strain at annealed areas. For this reason, a (422) reflection topograph was recorded with the sample oriented at the maximum strain position of the (422) rocking curve. This topograph is presented in Figure 1D. In this and subsequent topographs, areas of decreased x-ray intensity appear lighter with respect to the background, and areas of increased intensity appear darker. From the x-ray topographs, it is evident that some strain relief has occured at the centers of the majority of the laser annealed sites as shown by the lack of x-ray intensity. The dark rings around each site represent some form of strain transition region between the annealed and as-implanted areas. The exact cause for these rings will be discussed later.

The results from the (422) x-ray topograph provided firm evidence that some strain relief had occurred in the laser sites, and this motivated the detailed (400) rocking curve traverses which have been discussed earlier. The size of the x-ray beam (200 μm × 600 μm on the sample) used to obtain the (400) rocking curves was large compared to the size of some laser sites and there was considerable uncertainty (±300 μm) of position in the longitudinal direction of the x-ray beam. For these reasons, it is doubtful that the rocking curves in Figure 5 represent the centers of the annealed regions. Instead, for the smaller sites, they probably include some contribution from the partially strained transition regions and/or the as-implanted substrate.

The resolution of the nuclear emulsion plates used to record the x-ray topographs is considerably greater than can be attained by reducing the aperture of the x-ray beam used to record the rocking curves. It is more difficult to obtain quantitative information about strain from the topographs, but they compensate for this deficiency by simultaneously recording information from the whole surface of the sample.

In order to obtain as much information about the state of strain in the laser annealed sites, a series of (400) reflection topographs of the complete surface of the specimen were recorded at seven positions on the (400) rocking curve. The locations on the rocking curve at which topographs were recorded are shown in Figure 3 and the series of topographs are presented in Figure 11. X-ray topographs are typically recorded using reflections such as (422) (Fig. 1D) because the x-ray beam impinges on the sample at a very small angle ($\alpha = 1.5°$) and the diffracted beam exits nearly normal to the sample surface ($2\theta = 88°$). This allows the film plate to be placed very close to the sample without obstructing the incident x-ray beam and results in an undistorted image. The (400) reflection has a considerably less favorable geometry since $\alpha = \theta = 33°$ and $2\theta = 66°$. For this reason, there is distortion in the images in Figures 11 and 12. The amount of the distortion is not constant between topographs because the film plate was not positioned at exactly the same angle with respect to the specimen in each case.

It can be seen in Figures 11(1-6) that many of the laser-annealed sites have experienced strain relief since very little x-ray intensity has been recorded at the centers of these regions. With the exception of Figure 11(1), concentric dark/light ring-like features border these sites and probably represent incomplete strain relief or strain transition zones. Figures 11(1) and 1D both represent topographs taken at the maximum strain peak of the (400) and (422) rocking curves, respectively. Note that concentric ring-like features are present in the (422) topograph, but are absent in the equivalent (400) image. The (400) reflection is only sensitive to perpendicular strain within the sample since x rays are diffracted from lattice planes parallel with the surface. On the other hand, the (422) reflection contains information about both perpendicular and parallel strain since these lattice planes are included at an angle of 35.3° to the <100> surface. For this reason, the ring structures observed in the (422) topograph may be related to the state of parallel strain near the annealed sites.
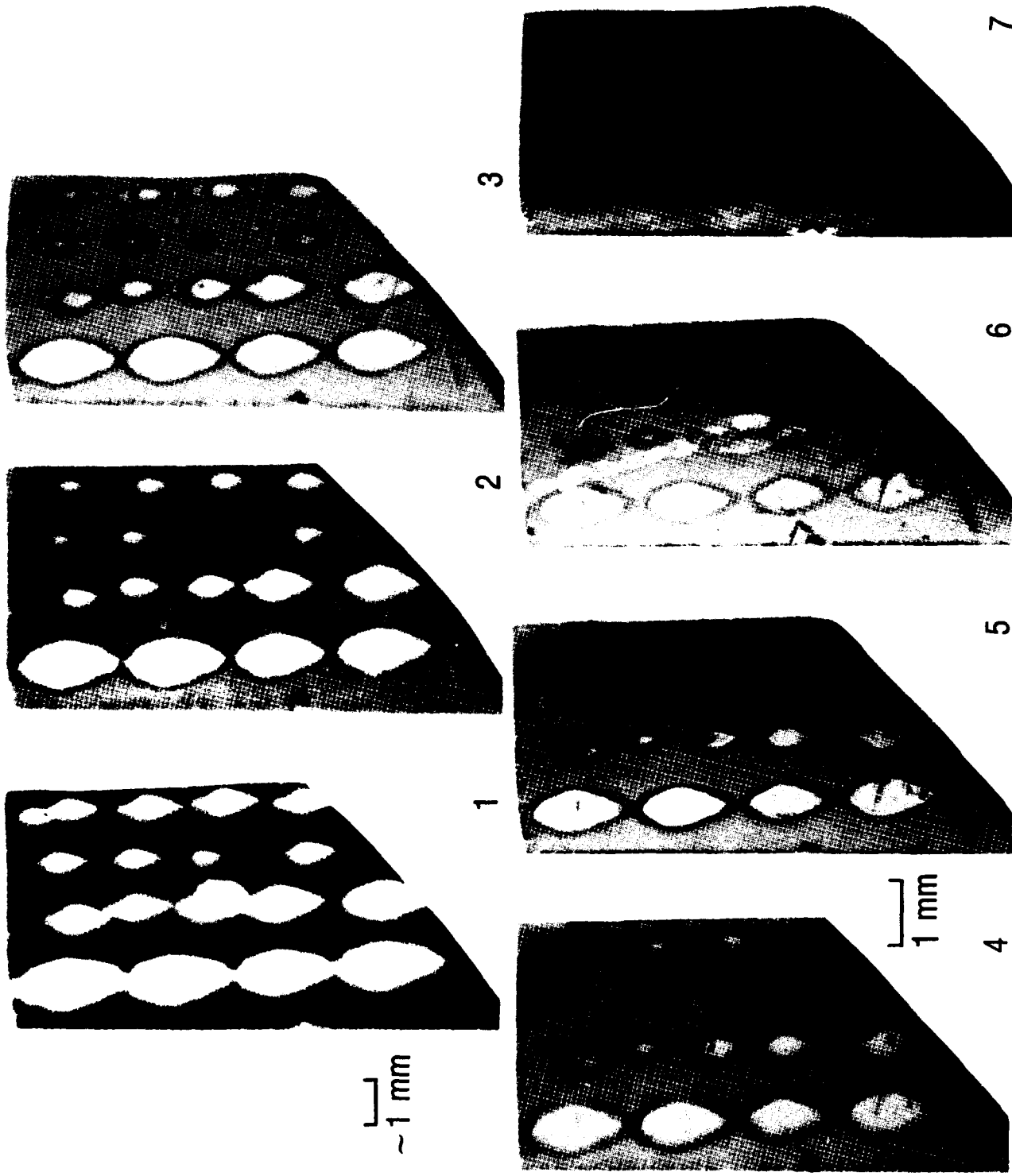
Figure 11. (400) Reflection Double-Crystal X-Ray Topographs Exposed at Various Positions on the Rocking Curve. See Figure 3 for positions corresponding to topographs.
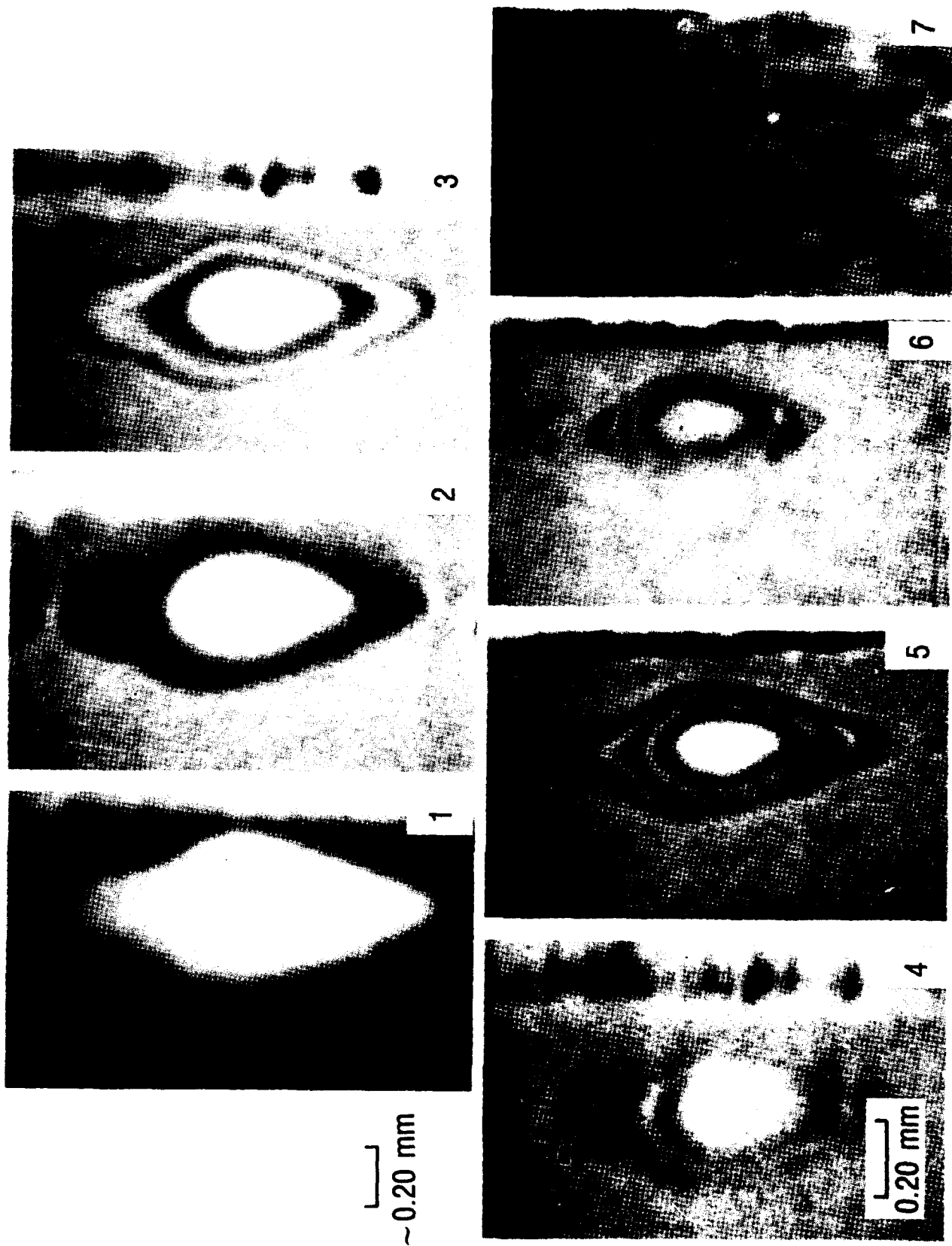
Figure 12. Enlargements of Laser Site 15 from (400) Reflection Double-Crystal X-Ray Topographs Exposed at Various Positions on the Rocking Curve. See Figure 11 for complete topographs.

A number of observations have been made concerning the features seen in the (400) topographs. These include: (1) the number of concentric bands is a minimum (0) at the highest strain position and increases (to a maximum of 3) as the strain position on the rocking curve decreases; (2) the size of the central strain relief zone decreases with decreasing strain; and (3) the broadest, most intense, concentric band is usually closest to the center of the relieved zone for all strain positions.

Table 1 summarizes the strain relief information obtained from the topographs for all laser sites, as a function of laser energy density and

Table 1. Summary of Strain Relief Information Obtained
from Topographs for All Laser Sites

		Position/ Perpendicular Strain (%)					
Site	Laser Energy Density (J/cm^2)	1 0.38	2 0.28	3 0.21	4 0.15	5 0.10	6 0.05
1	0.09	x	x	x	x	x	x
2	0.7	x	x	x	x	x	x
4	0.7	x	x	x	x	x	x
3	0.5	x	x	x	x	x	x
5	0.36	x	x	x	x	x	x
6	0.25	x	x	x	x	x	s?
7	0.18	x	x	x	x	x	s
9	0.12	x	x	x	x	x	s
15	0.12	x	x	x	x	s?	s
8	0.09	x	x	x	x	x	s
16	0.09	x	x	x	x	s?	s
17	0.08	x	x	x	s	s	s
10	0.08	x	x	x	s	s	s
11	0.06	x	x	x	s	s	s
14	0.06	x	x	x	s	s	s
18	0.06	x	x	s	s	s	s
12	0.045	x	x	s	s	s	0
13	0.045	x	x	x	s	s	s

x = Near complete strain relief in some portion of site with or
without strain transition bone (ring structures).
s = Some strain relief (change) indicated from ring structure.
0 = No change observed/indistinguishable from as-implanted region.

the strain at which relief has occurred. At the highest strain values
(> 0.28%) near complete strain relief has occurred at all laser sites
regardless of energy density (> 0.04 J/cm^2), whereas at the lowest
strain values (0.05%) only sites with laser energy densities greater than
0.25 J/cm^2 experienced complete relief of this strain.

The concentric ring structures observed in the topographs of the laser
sites have a somewhat unique appearance compared with other features seen
in x-ray topographs, and as a result, probably are formed by a unique
contrast-forming mechanism. The most common types of contrast in x-ray
topographs are due to extinction, lattice tilt, or lattice strain effects.
Extinction occurs in nearly perfect single crystals when the diffracted
x-rays tend to be doubly diffracted back towards the interior of the
crystal and destructively interfere with the incident x-ray beam. The
result is that a lower diffracted intensity is observed from nearly perfect
crystals than from less perfect crystals. The introduction of defects in a
nearly perfect crystal disrupts the extinction and produces an increased
diffracted intensity (extinction contrast). Since the surface of the GaAs
has been strained (and disordered) as a result of Si ion-implantation, it
is assumed that it no longer represents a nearly perfect single crystal and
that extinction effects are minimal.

Orientation contrasts due to lattice tilt and strain arise from local
areas in the crystal having slightly different orientation (tilt) or
lattice parameter (strain) than the bulk. This is equivalent to these
areas being at different positions on the rocking curve with respect to the
bulk, and they will exhibit increased or decreased intensity depending on
the sense of tilt or strain. Orientation contrast effects are often seen
in x-ray topographs at the margins of thin-film islands deposited on single
crystal substrates due to localized stresses in these areas (Refs. 11, and
12). From symmetry considerations, the sense of lattice tilt will be
reversed on opposite sides of film islands and this produces the opposite
sense of contrast in x-ray topographs. The same symmetry assumption would
also apply to the laser sites. Therefore, if significant lattice tilts are
present at the margins of the sites, they should have opposite senses on

29

opposite sides of the sites. As a result, the sense of the contrast (dark vs light) should be reversed in the x-ray topographs. The contrast features around the laser sites, however, are concentric and do not show contrast reversal; for this reason, it is felt that lattice tilts are not responsible for the contrast features.

Lattice strains do not display contrast reversal effects on opposite sides of film islands, but several factors indicate that this contrast mechanism is not responsible for the features observed in the x-ray topographs of the laser sites. Some of the laser sites display up to three dark concentric bands, but from a simple strain gradient only two dark contrast bands are possible (Ref. 12). Furthermore, in topographs of features such as film islands which display strain contrasts, a contrast minimum is observed at edges that are parallel with the incident x-ray beam. The features around the laser sites, however, display nearly constant contrast completely around the sites.

The concentric contrast features observed in the x-ray topographs of the laser sites do not appear to have been produced by the more common contrast forming mechanisms, but they do bear a striking resemblance to topographs of semiconductors that have experienced MeV ion-implantation (Refs. 13-16). For this reason, it is felt that this contrast (concentric bands) is produced by a similar mechanism.

Interference fringe features (concentric bands) have been observed in MeV ion-implanted semiconductors and a bi-crystal model has been proposed to account for these fringes (Refs. 13-16). MeV ion-implantation damages a crystal such that its surface is relatively unaffected, while at some depth (projected ion-range) the lattice has been amorphized or is high strained. Interference between x-rays diffracted by the bulk and undamaged surface produces the fringes observed in the x-ray topographs. This situation is similar to what is expected in some areas of the laser-annealed sites. The strain-depth profile modeled from the as-implanted regions (Fig. 3B) assumes that the surface of this sample is uniformly strained to a depth of

30

about 2500 Å, while at the center of laser-annealed sites the ion-implantation strain has been almost completely relieved. Neither of these cases represent a bi-crystal and no interference fringes are expected to be observed from these areas. Further from the center of the laser site it is assumed that strain relief has occurred at the surface, but that it has not progressed down to the undamaged bulk. These regions then approximate a bi-crystal and in these areas interference fringes are observed. This situation is represented schematically in Figure 13.

The interference nature of the fringes observed by other investigators (Refs. 15, 16) has been proven by recording and analyzing both reflection and transmission topographs from numerous different reflections. While this type of rigorous analysis has not been attempted in our case, the similarities between our observations and those from MeV ion-implantation support a common cause. In particular, both cases: (1) exhibit constant intensity around the fringes, (2) the number of observed fringes decreases as the position on the rocking curve, at which the topograph was taken, decreases from 0° delta theta, and (3) the strain-depth profiles are expected to have a similar form in areas that exhibit the fringes.

B.   RASTER ANNEALED GaAs

1.   X-RAY ROCKING CURVES

Figure 14A presents a (400) rocking curve obtained from an unannealed portion of the $5 \times 10^{15}/cm^2$ $^{28}Si^+$ ion implanted GaAs. In contrast with the $2 \times 10^{14}/cm^2$ implanted specimen, this sample has been strained up to a depth of 6000 Å with a maximum perpendicular strain of 0.50% (Figure 14B). By using the kinematical model of x-ray diffraction to match the oscillation periodicity and position of the lowest delta theta strain peak, the thickness of the strained layer and the maximum perpendicular strain, respectively, were obtained. The exact position of various strains within the sample are speculative.

A series of 20 (400) rocking curves were recorded at 0.625 mm intervals across the three raster anneal areas on the sample. Figures 15A and 15B represent a contour map and pseudo three-dimensional plot of x-ray rocking curve intensity compiled from these 20 scans. Individual rocking

31
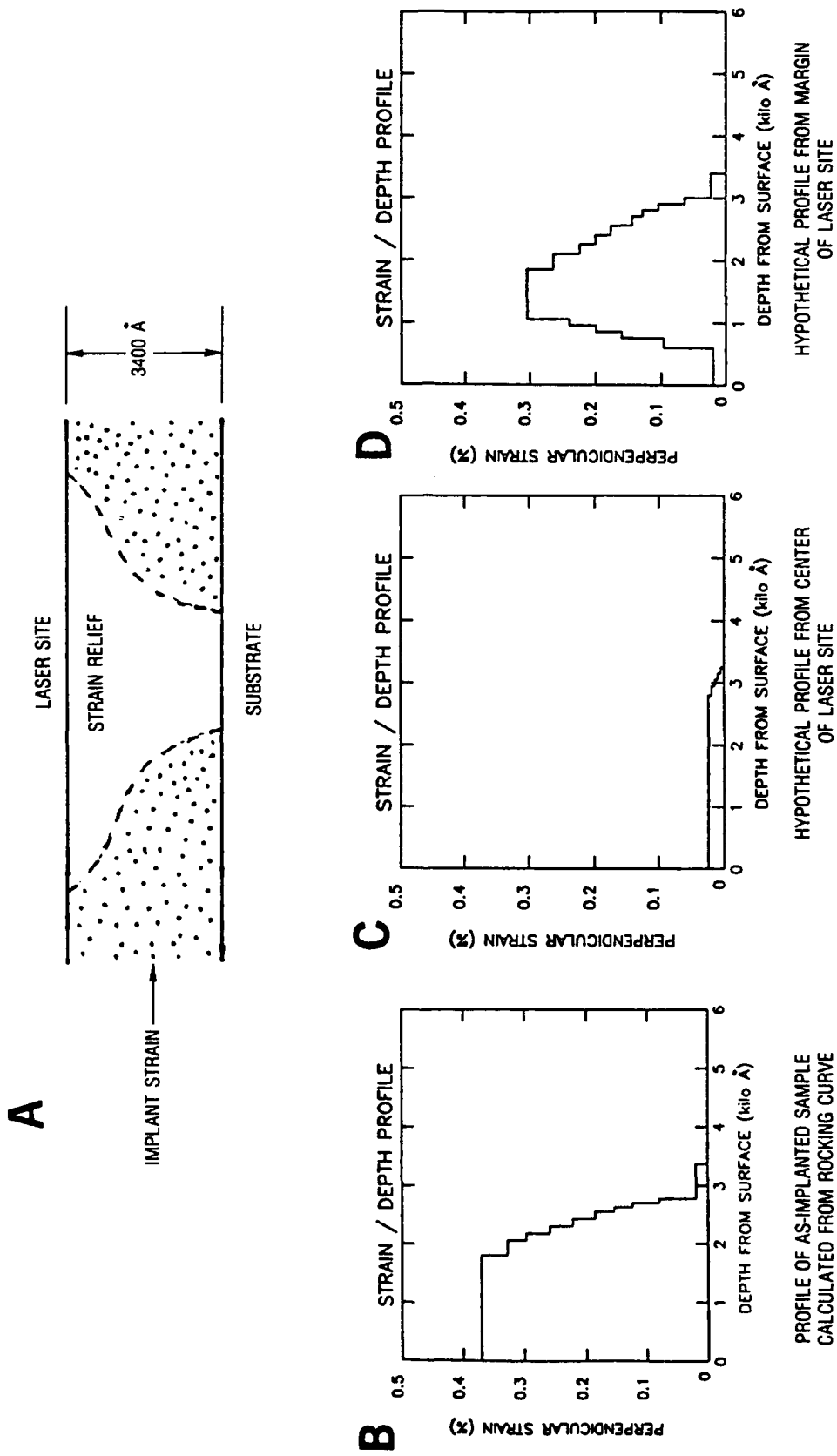
Figure 13.   (A) Schematic Cross Section of Laser Anneal Site;
(B) Calculated Strain/Depth Profile from As-Implanted Area;
(C,D) Hypothetical Profiles from Laser Anneal Site
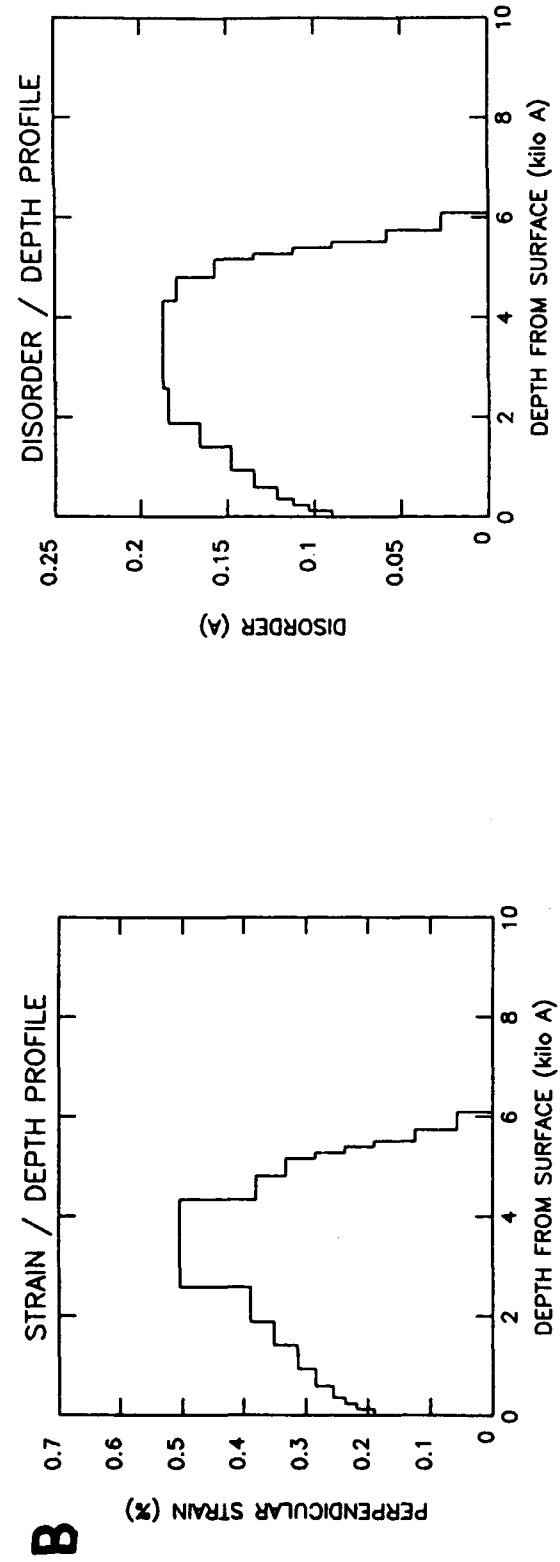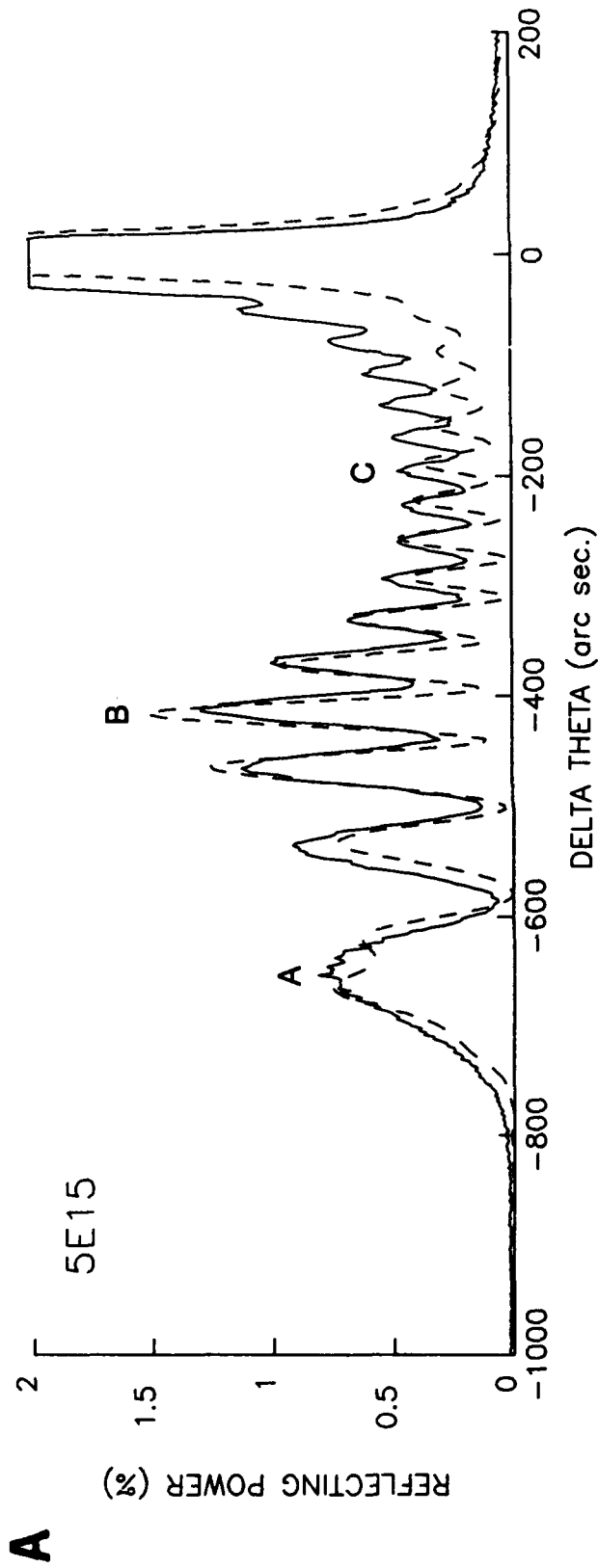
Figure 14A. Experimental and Calculated (400) Rocking Curves of 5 × 10^15/cm^2
180 keV ^28Si^+ As-Implanted GaAs.

Figure 15B. Strain and Disorder Depth Profiles Used to Provide the Calculated
Rocking Curve in Figure 14A.
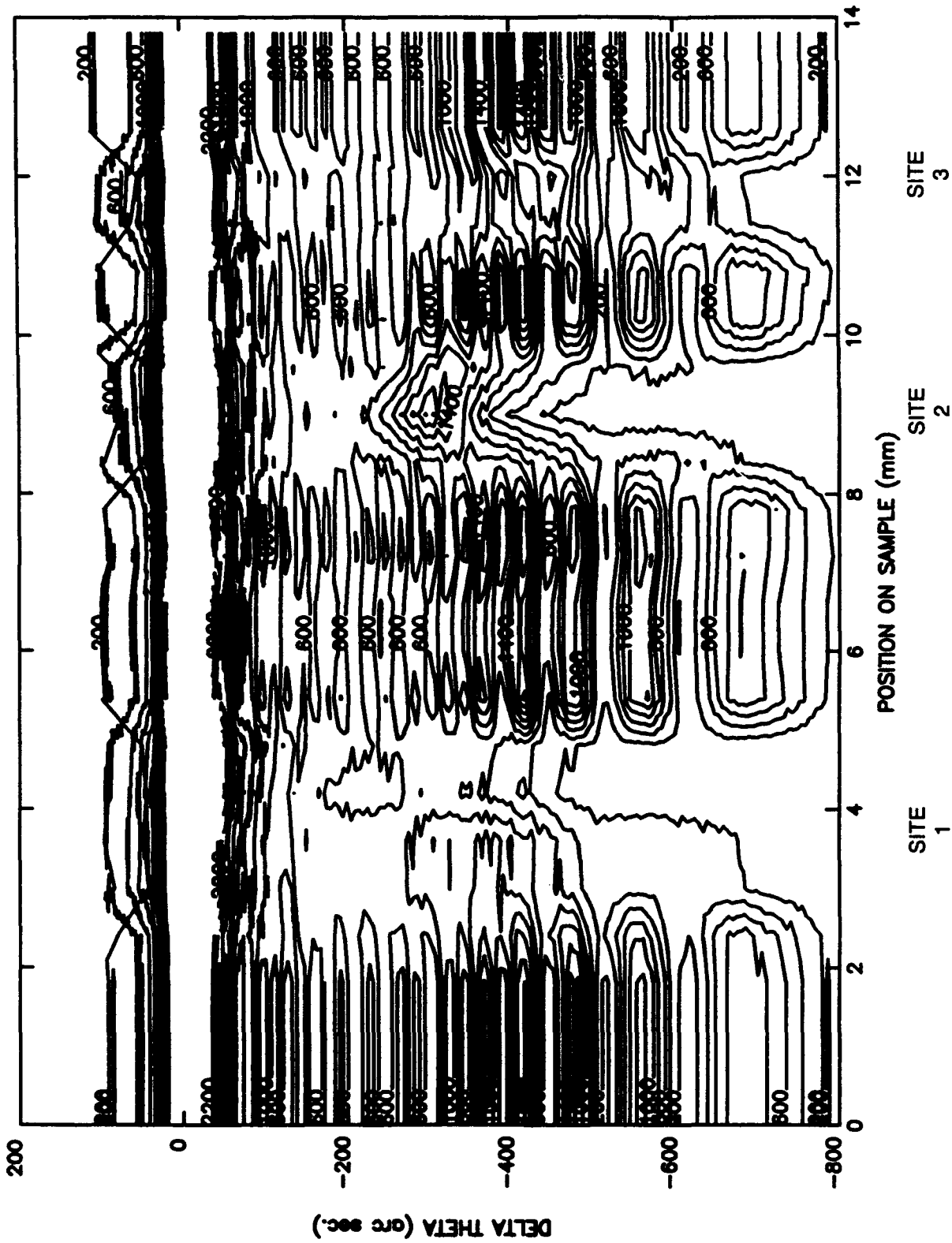
Figure 15A. (400) Reflection X-Ray Rocking Curve Intensity Contour Map Across Laser-Annealed Sites 1 to 3 on 5 × 10^{15}/cm^2 180 keV ^{28}Si$^+$ Implanted GaAs
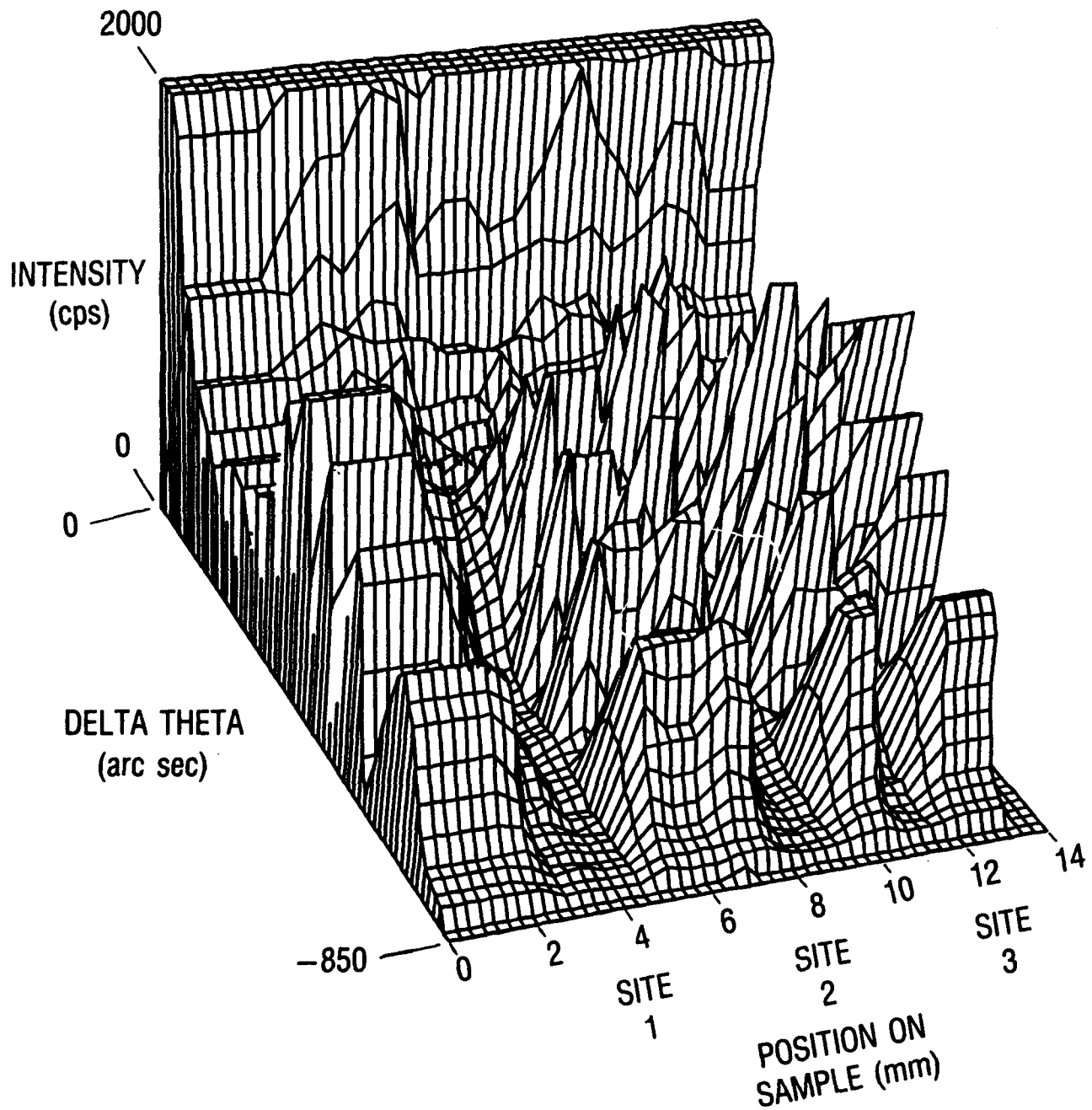
Figure 15B.   Pseudo Three-Dimensional (400) Rocking Curve Intensity
             Plot of Rastered Laser-Annealed $5 \times 10^{15}/cm^2$ 180 keV $^{28}Si^+$
             Ion-Implanted GaAs

curves of an unannealed area and the most strain-relaxed region of anneal
sites 1-3 are given in Figure 16A-D. From Figures 15 and 16, it can be
clearly seen that some strain relief has occurred at the laser annealed
sites. However, it is clear that the strain relief is far from complete,
since strain peaks on the negative side of the rocking curve are still
observed. The strain peak, at about -300 arc sec in the rocking curves of
sites 1 and 2, indicates that the same magnitude of strain is present in
both anneal sites and represents a perpendicular strain of about 0.22%.
The higher amplitude of this peak in the rocking curve from site 2, how-
ever, infers that the thickness of the strained layer is greater, or that
less disorder is present at this site. The rocking curve from site 3
displays two strain peaks at -400 and -600 arc sec delta theta, which
correspond to perpendicular strains of 0.45 and 0.30%, respectively. This
indicates that less strain relief has occurred at the site with the lowest
laser fluence.

2. DOUBLE-CRYSTAL X-RAY TOPOGRAPHY

The three (400) reflection x-ray topographs shown in Figure 17 were
taken at positions A, B, and C on the rocking curve in Figure 14A. At all
three sites, the highest as-implanted strain (0.50%) has been relieved, as
indicated by the absence of diffracted x rays. At sites 1 and 2, inter-
mediate levels of strain (>0.25%) have also been relieved; however, the
relaxation in site 2 is less uniform since individual anneal spots in the
raster pattern have become resolvable. These results are consistent with
the rocking curve data in Figure 16, since the rocking curves from sites 1
and 2 show no diffracted intensity at topograph positions A and B, whereas
that of site 3 has an intense peak at position B but no intensity at
position A. The interpretation of the topograph taken at position C on the
rocking curve is straightforward for sites 2 and 3. In these cases, the
intensity at this position on the rocking curve for sites 2 and 3 is nearly
equivalent to that for unannealed areas and, as a result, there is little
contrast associated with these areas in the topograph. The intensity at
position C in the rocking curve of site 1 is also similar to that of
unannealed areas.
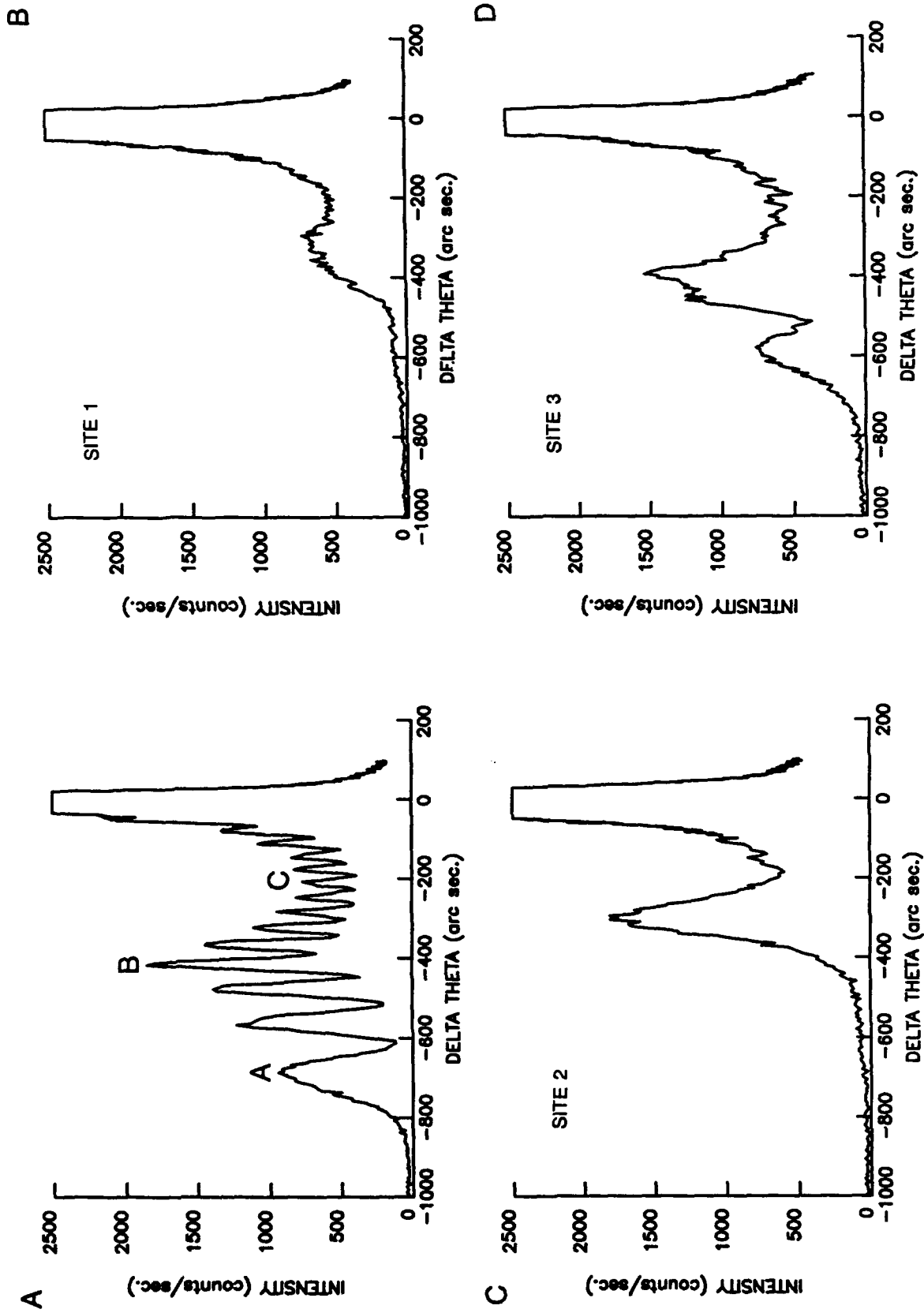
Figure 16. (400) Rocking Curves of $5 \times 10^{15}/cm^2$ $^{28}Si^+$ Ion-Implanted GaAs (A) and After Raster Laser Annealing at Site 1 (B), Site 2 (C), and Site 3 (D)

37
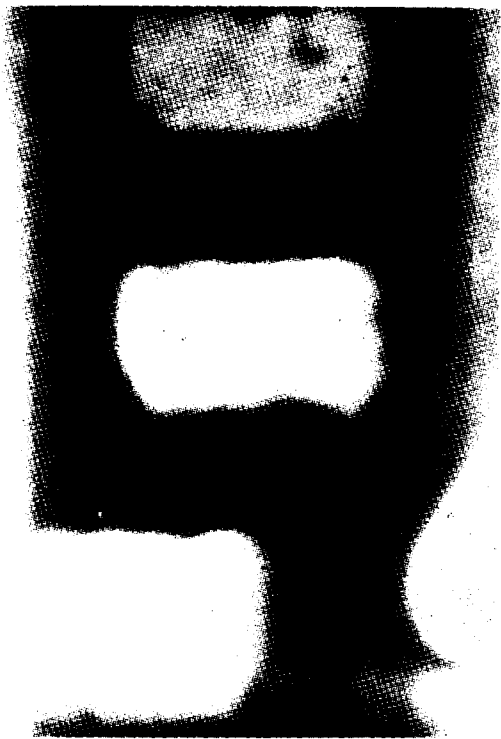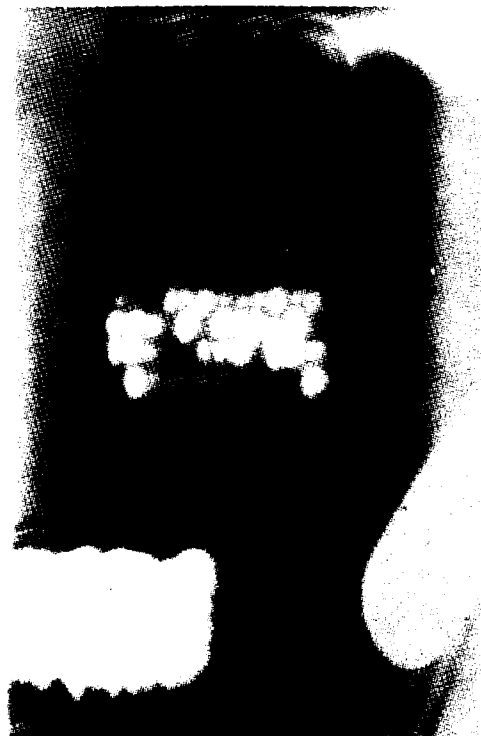
Figure 17. (400) Reflection X-Ray Topographs Taken at Positions A-C on the Rocking Curve in Figure 14a

However, there is very high contrast and nonuniformity associated with this site on the topograph. This nonuniformity may account for the appearance of the rocking curve if the x-ray beam happened to sample areas of both increased and decreased diffracted intensity.

Interference fringe-like features are also visible in the x-ray topographs of the raster-annealed sample, and it is assumed that they have a similar origin as those observed in topographs of the single-laser, spot-annealed sample. However, the interpretation of these fringes in this case is complicated by the multispot raster-annealing pattern becoming resolvable in topographs taken at lower levels of strain.

IV. SUMMARY

Double-crystal x-ray rocking curves and topographs have been used to study the relief of strain in $^{28}Si^+$ ion-implanted GaAs produced by pulsed laser annealing. X-ray rocking curves of the 140 keV $2 \times 10^{14}/cm^2$ as-implanted GaAs indicated that the upper 2000 Å of the sample had been strained to a maximum of 0.38%. Rocking curves of two of the laser-annealed sites with the highest energy densities (and largest areas of annealing) indicated that the ion-implantation strain at each had been almost completely relieved, but the relief could not be correlated with an increase in intensity of the unstrained peak. Results from lower energy density annealed sites were less conclusive because of uncertainties in positioning the x-ray beam in the exact center of small sites.

X-ray rocking curves of the 180 keV $5 \times 10^{15}/cm^2$ as-implanted sample revealed that it was strained to a maximum of 0.50% with strain extending to 6000 Å beneath the surface. Rocking curves from all three of the raster-annealed sites indicated the presence of residual strains as high as 0.45% and 0.22% for the lowest and highest laser fluences, respectively.

Double-crystal reflection x-ray topographs of the spot-annealed sample, taken at various positions on the rocking curve, were able to qualitatively map out the state of strain to much higher resolution than the x-ray rocking curves. Laser energy densities of greater than approximately 0.25 J/cm^2 were able to relieve nearly all of the ion-implantation strain in at least some portion of the sites, whereas all laser energy densities were able to relieve strains of above 0.21% in some portions of the sites. The x-ray topographs of the laser sites exhibited unusual interference fringe patterns that have been attributed to a bi-crystal structure produced in some areas of the laser annealed areas.

X-ray topographs of the raster-annealed sample generally agreed with individual rocking curves from the anneal sites. In this specimen, laser fluences, which produced near total strain relief in the 140 keV $2 \times 10^{14}/cm^2$ sample, left considerable residual strains. This is probably more a result

41

of the greater total thickness of the strained layer (6000 Å vs 3800 Å), rather than the higher as-implanted strain, since if there were insufficient heating (melting?) at the strained layer to substrate interface, then the unstrained substrate could not serve as a perfect seed for complete strain relief.

REFERENCES

1. H. Yao, <u>Optical Studies of Extremely Heavily Doped n-GaAs Produced by Pulsed-Laser Annealing</u>, Ph.D Dissertation, Kansas State University (1989).

2. R. C. Bowman, Jr., T. F. Knudsen, P. M. Adams, H. D. Yao, and A. D. Compaan, "X-Ray and Raman Topographic Studies of GaAs Implanted with ^{28}Si and Pulsed Laser Anneal," <u>Mat. Res. Soc. Symp. Proc.</u> (1990) (in press).

3. V. Speriosu, B. Paine, M. Nicolet, and H. Glass, "X-Ray Rocking Curve Study of Si-Implanted GaAs, Si, and Ge," <u>Appl. Phys. Lett.</u> <u>40</u> 604-606 (1982).

4. B. Paine and V. Speriosu, "Non-Linear Strain Effects in Ion-Implanted GaAs," <u>J. Appl. Phys.</u> <u>62</u>, 1704-1705 (1987).

5. B. Paine, N. Hurvitz, and V. Speriosu, "Strain in GaAs by Low Dose Ion Implantation," <u>J. Appl. Phys.</u> <u>61</u>, 1335-1339 (1987).

6. G. Bai, D. Jamieson, M. Nicolet, and T. Vreeland, "Defects Annealing of Si$^+$ Implanted GaAs at RT and 100°C," <u>Mat. Res. Soc. Symp. Proc.</u> <u>93</u>, 67-72 (1987).

7. V. S. Speriosu, "Kinematical X-Ray Diffraction in Nonuniform Crystalline Films, Strain and Damage Distribution in Ion-Implanted Garnets," <u>J. Appl. Phys.</u> <u>52</u>, 6094-6103 (1981).

8. W. Hubrig, J. Auleytner, and M. Maciaszek, "Changes of X-Ray Topographic Contrast Due to Annealing of Boron-Implanted Silicon," <u>Phys. Stat. Sol. (A)</u> <u>36</u>, 205-215 (1976).

9. B. Larson and J. Barhost, "X-Ray Study of Lattice Strain in Boron Implanted Laser Annealed Silicon," <u>J. Appl. Phys.</u> <u>51</u>, 3181-3185 (1980).

10. R. D. Dragsdurf and C. P. Bhalla, "X-Ray Topography of Ion-Implanted Laser Annealed Si," in <u>Advances in X-Ray Analysis</u>, Vol. 29, C. Barrett et al., eds. (1986), pp. 381-386.

11. G. Schwuttke and J. Howard, "X-Ray Stress Topography of Thin Films on Germanium and Silicon," <u>J. Appl. Phys.</u> <u>39</u>, 1581-1591 (1968).

12. P. Adams, "Quantification of Strain and Lattice Deformation in Single Crystals," ATM-88(8325)-1, The Aerospace Corporation (23 September 1988).

13. H. Tekaat and G. Schwuttke, "X-Ray Double Crystal Diffractometer Investigations of Implanted Silicon: D^+ and N^+" in <u>Advances In X-Ray Analysis</u>, Vol. 15, K. Heinrich et al., eds. (1972), pp. 504-515.

14. K. Brack, E. Gurey, and G. Schwuttke, "Damage Profiles in High Energy C^+ Bombarded Silicon," <u>Crystal Lattice Defects</u> <u>4</u>, 109-121 (1973).

15. V. Bonse, M. Hart, and G. Schwuttke, "X-Ray Investigation of Lattice Deformations in Silicon Induced Through High Energy Ion Implantation," <u>Phys. Stat. Sol</u>. <u>33</u>, 361-374 (1969).

16. K. Wietesca, "X-Ray Diffraction Investigations of High Energy α-Particle Damage in Silicon," <u>Phys. Stat. Sol. (A)</u> <u>68</u>, 179-185 (1981).

LABORATORY OPERATIONS

The Aerospace Corporation functions as an "architect-engineer" for national security projects, specializing in advanced military space systems. Providing research support, the corporation's Laboratory Operations conducts experimental and theoretical investigations that focus on the application of scientific and technical advances to such systems. Vital to the success of these investigations is the technical staff's wide-ranging expertise and its ability to stay current with new developments. This expertise is enhanced by a research program aimed at dealing with the many problems associated with rapidly evolving space systems. Contributing their capabilities to the research effort are these individual laboratories:

Aerophysics Laboratory: Launch vehicle and reentry fluid mechanics, heat transfer and flight dynamics; chemical and electric propulsion, propellant chemistry, chemical dynamics, environmental chemistry, trace detection; spacecraft structural mechanics, contamination, thermal and structural control; high temperature thermomechanics, gas kinetics and radiation; cw and pulsed chemical and excimer laser development, including chemical kinetics, spectroscopy, optical resonators, beam control, atmospheric propagation, laser effects and countermeasures.

Chemistry and Physics Laboratory: Atmospheric chemical reactions, atmospheric optics, light scattering, state-specific chemical reactions and radiative signatures of missile plumes, sensor out-of-field-of-view rejection, applied laser spectroscopy, laser chemistry, laser optoelectronics, solar cell physics, battery electrochemistry, space vacuum and radiation effects on materials, lubrication and surface phenomena, thermionic emission, photosensitive materials and detectors, atomic frequency standards, and environmental chemistry.

Electronics Research Laboratory: Microelectronics, solid-state device physics, compound semiconductors, radiation hardening; electro-optics, quantum electronics, solid-state lasers, optical propagation and communications; microwave semiconductor devices, microwave/millimeter wave measurements, diagnostics and radiometry, microwave/millimeter wave thermionic devices; atomic time and frequency standards; antennas, rf systems, electromagnetic propagation phenomena, space communication systems.

Materials Sciences Laboratory: Development of new materials: metals, alloys, ceramics, polymers and their composites, and new forms of carbon; nondestructive evaluation, component failure analysis and reliability; fracture mechanics and stress corrosion; analysis and evaluation of materials at cryogenic and elevated temperatures as well as in space and enemy-induced environments.

Space Sciences Laboratory: Magnetospheric, auroral and cosmic ray physics, wave-particle interactions, magnetospheric plasma waves; atmospheric and ionospheric physics, density and composition of the upper atmosphere, remote sensing using atmospheric radiation; solar physics, infrared astronomy, infrared signature analysis; effects of solar activity, magnetic storms and nuclear explosions on the earth's atmosphere, ionosphere and magnetosphere; effects of electromagnetic and particulate radiations on space systems; space instrumentation.